Study of Photorefractive Dynamics in Poly(triarylamine)-based Polymer Composites

Kento Masumura

Department of Materials Chemistry
Kyoto Institute of Technology

March 2019

Content

Chapter 1: Introduction

1.1. Introduction

The PR phenomenon was reported in the inorganic crystals of lithium niobate ($LiNbO_3$) and lithium tantalate ($LiTaO_3$) by Ashkin et al. in 1966; light scattering in these crystals became stronger with the passage of time by irradiating the laser beam, and this phenomenon was first interpreted as an optical damage of the crystals [1]. However, the light scattering was disappeared after turning off the light and reproducibility was also confirmed. Chen et al. reported a hologram recording using this effect in 1968 [2], and they suggested a model to explain the refractive index modulation in 1969 [3]. After that, this phenomenon has been called "photorefractive effect" and founded in many electro-optic crystals. In 1978, Kukhtarev et al. proposed a standard model of the current PR effect by analyzing the beam coupling of the refractive index modulation grating formed by the PR effect [4, 5]. The photorefractive (PR) effect is defined as spatial modulation of the index of refraction due to charge redistribution in a nonlinear optical material [6]. The PR effect is based on a refractive index modulation grating, whose phase is shifted by Φ from the light and dark pattern due to the interference of the light. Resulting from the phase shift, asymmetric energy transfer, called two-beam (TBC) coupling occurs and optical amplification effect is induced.

Many researches on $LiTaO_3$ and many other inorganic crystals have been widely reported since the PR effect was discovered. Moerner et al. developed a PR material using organic and polymer materials in 1991 [7]. Advantages of using organic and polymer materials for PR materials are as follows: they have several features, excellent processability in the form of large area films, wide selectivity of materials including relatively inexpensive ones, adjustable performances, and large space charge electric field due to low permittivity [8]. For these reasons, they have attracted wide attention for the practical applications of holographic 3D displays.

The PR phenomenon in PR polymeric composites involves the following processes: (1) photoexcitation produces charge carriers in the bright region of the interference pattern, (2) the produced charge carriers (mainly holes) are transported through the PR material along an external applied electric field until they are trapped in the dark region of the interference pattern, (3) a space-charge field is formed periodically between trapped holes and the remaining electrons, and (4) the refractive index modulation is induced by both the electro-optic (Pockels) effect and the reorientation of the nonlinear optical (NLO) dye [9, 10]. These processes result in the optical diffraction and the optical amplification. A normal photorefractive crystal represented by $LiTaO_3$ has weak diffraction, whereas the photorefractive polymer composites commonly exhibit high diffraction efficiency because of the orientational enhancement effect induced by the NLO chromophore. Therefore, the holographic characteristics of high diffraction efficiency and short response time for the photorefractive polymer composites are attractive for realistic 3D displays [11]. The high diffraction efficiency is related to the

contrast of the holographic images, and the short response time is relevant to the smooth motion of the holographic images. The fast response of the optical amplification is also attractive for applications in telecommunications.

PR studies of organic and polymer materials presented the millisecond order response time [12], nearly 100% diffraction efficiency [13], as well as gain factor above 400 cm^{-1} [14]. In recent years, PR properties using molecular glasses [15, 16], PR composites incorporating electron trapping agents [17, 18], and PR properties in infrared region using two-photon absorption [19, 20] were reported. To develop the PR effect in the organic and polymeric material, externally applied electric field of 10^1 – 10^2 $V\mu m^{-1}$ is required to drift the holes. The time required for the formation of the refractive index modulation grating is commonly in the order of seconds in the inorganic crystals, while it is in the order from seconds to milliseconds in the organic and polymeric materials.

From such a viewpoint, the PR performances have been investigated using poly (*N*-vinyl carbazole) (PVCz, or PVK) with different molecular weights [21, 22], using polymers with different carbazole derivatives [23], and using PVCz with various sensitizers [24]. These studies were aimed to improve the performances using carbazole-based PR materials. In recent years, numerous studies have focused on improving the response time using the methyl-substituted poly(triarylamine)-derived polymers with a high hole mobility ($\mu = 10^{-2}$ cm^2 V^{-1} s^{-1}) [25, 26]. Based on these reports, various new applications such as optical amplification and phase conjugate wave generation are expected as new photonics materials.

1.2. Research Objectives

For the practical use of PR polymer materials, high diffraction efficiency and fast response speed are indispensable. Application to a holographic display as a moving image requires a response time less than the video rate (30 Hz, 33 ms) and a diffraction efficiency of 50% or more. In recent years, many PR polymer materials having high diffraction efficiency satisfying these requirements have been reported, but there are few reports on PR polymer materials having response time faster than the video rate. Furthermore, there is a trade-off relationship between the diffraction efficiency and the response time in general, and to overcome the trade-off is one of the biggest issues for practical application.

In recent years, triphenylamine polymers with high carrier mobility have been introduced as photoconductive polymers in this laboratory to fabricate the PR materials with high speed response in 2005 [27]. In 2012, a side chain type triphenylamine polymer, poly(4-diphenylamino)styrene (PDAS) ($\mu = 10^{-4}$-10^{-3} cm^2 V^{-1} s^{-1}), achieving a response time of 39 ms and succeeded in real time rewriting of holograms [28]. Furthermore, in 2013, a main chain type triphenylamine polymer, poly[bis(2, 4, 6-trimethylphenyl) amine] (PTAA) ($\mu = 10^{-3}$-10^{-2} cm^2 V^{-1} s^{-1}), having higher charge carrier mobility than

PDAS by modifying ITO substrates with self-assembled monolayer (SAM) was reported [29].

In this research, further improvement of the PR performance is aimed using PTAA, showing sub-millisecond order response time. In a previous study, a response time of 11 ms and a diffraction efficiency of 3% were obtained with an applied electric field of 20 V μm^{-1} [29]. To enhance these PR performances, higher electric field is commonly required. Since PTAA has high mobility in the order of 10^{-3}-10^{-2} cm^2 V^{-1} s^{-1} and low HOMO (highest occupied molecular orbital) level of -5.2 eV, high photocurrent flows at an applied voltage of 30 V μm^{-1} or more, inducing easy dielectric breakdown. Therefore, to control the photocurrent adequately is the main issue for the PTAA-based PR composites. For this objective, the optimization of PTAA composite materials was undertaken by changing the type and weight ratio of plasticizer and sensitizer. Furthermore, in order to avoid the dielectric breakdown when a short wavelength light source is used, second electron trapping agents are introduced.

1.3. Outline of the thesis

This thesis consists of six chapters. General introduction is in chapter 1. Experimental methods are described in chapter 2. As a first modification of the PTAA-based PR composite, the content of sensitizer is optimized in chapter 3. The wavelength dependence of the PR parameters in the PTAA-based PR composite is also discussed in chapter 3. In chapter 4, various second electron acceptors are investigated to suppress the photocurrent of the PR composite. Further optimization to maximize the sensitivity by the reduction of the absorbance of the PTAA-based PR composite is described in chapter 5. Finally, the contents of the thesis are summarized in chapter 6.

1.4. Photorefractive effect

1.4.1. Photorefractive effect

The photorefractive (PR) effect is an optical phenomenon, in which the refractive index is locally modulated by the spatial distribution of the light intensity. As the same as in the inorganic crystal, in which the PR effect is induced by irradiating interfered two coherent lights to a crystal having electrooptic effect such as ferroelectric oxide crystals, the organic materials with photoconductive and second-order nonlinear optical properties induce the space charge distribution corresponding to the light intensity distribution when irradiating by the interfered two coherent light under applying an external electric field. This phenomenon is caused by the periodic induction of the refractive index modulation through the Pockels effect, which is the second-order nonlinear optical effect (first order electrooptic effect).

For the PR effect in the organic and polymeric materials, photoconductivity for generating charge carriers and Pockels effect as a primary electrooptic effect causing the refractive index modulation are required. The orientational enhancement effect due to molecular orientation of nonlinear optical (NLO) molecules also has a great influence on PR performances.

1.4.2. Photoconductivity

Photoconductivity is a phenomenon that the electrical conductivity increases when the light is irradiated to an insulator or a semiconductor. This phenomenon has been investigated in various substances such as organic crystals and polymers with a large conjugated π electron systems, for example, carbazole type moiety exhibiting excellent photoconductivity. Photoconductivity has carrier generation process, carrier transfer process, carrier trapping, and recombination process. Generally, carriers are generated by photoexcitation, and carriers are drifted along an applied electric field.

1.4.3. Electro-optic effect

The primary electro-optic effect (Pockels effect) is a phenomenon in which the refractive index is proportional to the intensity of the electric field modulated by the redistributed space charge field, when an electric field is applied to the materials having a second-order optical nonlinearity. The non-zero Pockels effect is in the presence of the random orientation of the nonlinear optical molecule or a centrosymmetric structure. Therefore, it is required to have a non-centrosymmetric structure and the macroscopically orienting dipoles in the medium in a certain direction by poling or the like.

1.4.4. Orientational enhancement effect

In inorganic materials, the electro-optical effect is dominant factor for the refractive index modulation. On the other hand, in organic and polymeric materials, the molecular orientation of nonlinear optical (NLO) molecules is additionally effective. This effect is called an orientational enhancement effect.

1.4.5. Mechanism of photorefractive effect in organic and polymeric materials

The PR effect of organic and polymeric materials are summarized as follows:

(1) Spatial modulation of intensity in a medium is formed by interfering two coherent laser beams. In the bright area of the optical interference pattern, charge carriers are produced by the photoexcitation.

(2) Charge carriers (holes in this study) produced in the bright area are drifted along the external applied electric field and trapped at the dark area.

(3) Spatial electric field is formed between charge carriers (hole) trapped in the dark area and the remained electrons in the bright area.

(4) The formed spatial electric field and the external applied field induce a Pockels effect, a first-order electrooptic effect, and a refractive index modulation grating is induced. Along the fringe pattern of intensity, the refractive index modulation is periodically formed in the substances. Refractive index modulation causes the holographic optical diffraction in the substances. A spatial phase difference Φ is generated between the refractive index modulation grating and the optical interference fringes. This phase difference induces the optical amplification due to asymmetric energy transfer, which is unique properties of PR effect.

(5) Further, the nonlinear optical dye is oriented by the formed spatial electric field, additionally inducing larger refractive index modulation (orientational enhancement effect).

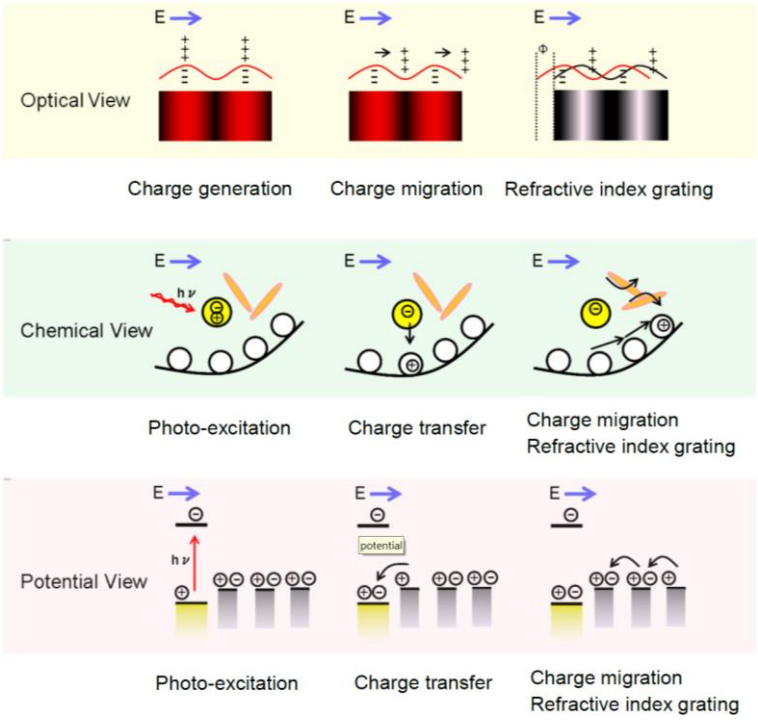

Figure 1.1. Mechanism for photorefractive effect.

References and links

[1] A. Ashkin, G. D. Boyd, J. M. Dziedzic, R. G. Smith, A. A. Ballman, J. J. Levinstein and K. Nassau, "Optically-induced refractive index inhomogeneities in $LiNbO_3$ and $LiTaO_3$," *Appl. Phys. Lett.* **9**(1), 72-73 (1966).

[2] F. S. Chen, J. T. LaNacchia and D. B. Fraser, "Holographic strage in lithium niobite," *Appl. Phys. Lett.* **13**(7), 223-224 (1968).

[3] F. S. Chen, "Optically Induced Change of Refractive Indices in $LiNbO_3$ and $LiTaO_3$," *J. Appl.Phys.* **40**(8), 3389-3396 (1969).

[4] N. V. Kukhtarev, V. B. Markov, S. G. Odulov, M. S. Soskin and V. L. Vinetskii, "Holographic storage in electrooptic crystals. i. steady state," *Ferroelectrics* **22**(1), 949-960 (1978).

[5] N. V. Kukhtarev, V. B. Markov, S. G. Odulov, M. S. Soskin and V. L. Vinetskii, "Holographic storage in electrooptic crystals. II. beam coupling—light amplification," *Ferroelectrics* **22**(1), 961-964 (1978).

[6] P. Günter and J. P. Huignard, "Photorefractive Materials and Their Applications II," *Spronger-Verlag* (1988).

[7] S. Ducharme, J. C. Scott, R. J. Twieg and W. E. Moerner, "Observation of the photorefractive effect in a polymer," *Phys. Rev. Lett.* **66**(14), 1846-1849 (1991).

[8] S. Köber, M Salvadorand K Meerholz, "Organic Photorefractive Materials and Applications," *Adv. Mater.* **23**(41), 4725-4763 (2011).

[9] W. E. Moerner and S. M. Silence, "Polymeric photorefractive materials," *Chem. Rev.* **94**(1), 127-155 (1994).

[10] B. Lynn, P. –A. Blanche and N. Peyghambarian, "Photorefractive polymers for holography," *J. Polym. Sci., B, Polym. Phys.* **52**(3), 193–231 (2014).

[11] S. Tay, P. A. Blanche, R. Voorakaranam, A. V. Tunç, W. Lin, S. Rokutanda, T. Gu, D. Flores, P. Wang, G. Li, P. St Hilaire, J. Thomas, R. A. Norwood, M. Yamamoto and N. Peyghambarian, "An updatable holographic three-dimensional display," *Nature* **451**(7179), 694–698 (2008).

[12] D. Wright, M. A. Diaz-Garcia, J. D. Casperson, M. DeClue, W. E. Moerner and R. J. Twieg, "High-speed photorefractive polymer composites," *Appl. Phys. Lett.* **73**(11), 1490-1492 (1998).

[13] K. Meerholtz, B. L. Volodim, Sandalphon, B. Kippelen and N. Peyghambarian, "A photorefractive polymer with high optical gain and diffraction efficiency near 100%," *Nature* **371**(6497), 497-500 (1994).

[14] O. Ostroverkhova and W. E. Moerner, "High-performance photorefractive organic glass with near-infrared sensitivity," *Appl. Phys. Lett.* **82**(21), 3602-3604 (2003).

[15] P. M. Lundquist, R. Wortmann, C. Geletneky, R. J. Twieg, M. Jurich, V. Y. Lee, C. R. Moylan and D. M. Burland, "Organic Glasses: A New Class of Photorefractive Materials," *Science* **274**(5290), 1182-1185 (1996).

[16] N. Tsutsumi, J. Eguchi and W. Sakai, "High performance photorefractive molecular glass composites in reflection gratings," *Chem. Phys. Lett*. **408**(4-6), 269-273 (2005).

[17] W. You, Z. Hou and L. Yu, "Dramatic Enhancement of Photorefractive Properties by Controlling Electron Trap Density in a Monolithic Material," *Adv. Mater*. **16**(4), 356-360 (2004).

[18] J. Zhang, Z. Chen, Y. Liu, M. Huang, Q. Wei and Q. Gong, "Improvement on the photorefractive performance of a monolithic molecular material by introducing electron traps," *Appl. Phys. Lett.* **85**(8), 1323-1325 (2004).

[19] S. Tay, J. Thomas, M. Eralp, G. Li, B. Kippelen, S. R. Marder, G. Meredith, A. Schülzgen and N. Peyghambarian, "Photorefractive polymer composite operating at the optical communication wavelength of 1550 nm," *Appl. Phys. Lett.* **85**(20), 4561-4563 (2004).

[20] S. Tay, J. Thomas, M. Eralp, G. Li, R. A. Norwood, A. Schülzgen, M. Yamamoto, S. Barlow, G. A. Walker, S. R. Marder and N. Peyghambarian, "High-performance photorefractive polymer operating at 1550 nm with near-video-rate response time," *Appl. Phys. Lett.* **87**(17), 171105 (2005).

[21] N. Tsutsumi and H. Kasaba, "Effect of molecular weight of poly(*N*-vinyl carbazole) on photorefractive performances," *J. Appl. Phys.* **104**(7), 073102 (2008).

[22] N. Tsutsumi and Y. Shimizu, "Asymmetric Two-Beam Coupling with High Optical Gain and High Beam Diffraction in External-Electric-Field-Free Polymer Composites," *Jpn. J. Appl. Phys*. *Part 1* **43**(6A), 3466-3478 (2004).

[23] N. Tsutsumi and W. Miyazaki, "Photorefractive performance of polycarbazoylethylacrylate composites with photoconductive plasticizer," *J. Appl. Phys.* **106**(8), 083113 (2009).

[24] N. Tsutsumi, Y. Ito and W. Sakai, "Effect of sensitizer on photorefractive nonlinear optics in poly(*N*-vinylcarbazole) based polymer composites," *Chem. Phys.* **344**(1-2), 189-194 (2008).

[25] P. A. Bobbert, A. Sharma, S. G. J. Mathijssen, M. Kemerink and D. M. de Leeuw, "Operational Stability of Organic Field‐Effect Transistors," *Adv. Mater.* **24**(9), 1146-1158 (2012).

[26] J. Smith, W. Zhang, R. Sougrat, K. Zhao, R. Li, D. Cha, A. Amassian, M. Heeney, I. McCulloch and T. D. Anthopoulos, "Solution‐Processed Small Molecule‐Polymer Blend Organic Thin‐Film Transistors with Hole Mobility Greater than 5 cm^2/Vs" *Adv. Mater.* **24**(18), 2441-2446 (2012).

[27] N. Tsutsumi, T. Murao and W. Sakai, "Photorefractive Response of Polymeric Composites with Pendant Triphenylamine Moiety," *Macromol.* **38**(17), 7521-7523 (2005).

[28] S. Tsujimura, K. Kinashi, W. Sakai and N. Tsutsumi, "High-Speed Photorefractive Response Capability in Triphenylamine Polymer-Based Composites," *App. Phys. Express* **5**(6), 064101 (2012).

[29] K. Kinashi, H. Shinkai, W. Sakai and N. Tsutsumi, "Photorefractive device using self-assembled monolayer coated indium-tin-oxide electrodes," *Org. Electron.* **14**(11), 2987–2993 (2013).

Chapter 2: Experimental section

2.1. Materials and composite preparation

2.1.1. Materials

Poly[bis(4-phenyl)(2,4,6-trimethylphenyl)amine] (PTAA) was purchased from Sigma-Aldrich and used as a photoconductive polymer. Piperidinodicyanostyrene (PDCST) as a nonlinear optical (NLO) dye and (2,4,6-trimethylphenyl)diphenylamine (TAA) as a plasticizer were synthesized using procedures described in the next section 2.1.2. [6,6]-Phenyl-C61- butyric acid methyl ester (PCBM) was purchased from Tokyo Kasei and used as a sensitizer. Tris(8-hydroxyquinolinato)aluminium (Alq_3), 1,3-bis[2-(4-*tert*-butylphenyl)-1,3,4-oxadiazo-5-yl]benzene (OXD-7) or bathophenanthroline (BPhen) were also bought from Tokyo Kasei and used as second electron traps. Structural formulae of these materials are shown in Figure 2.1.

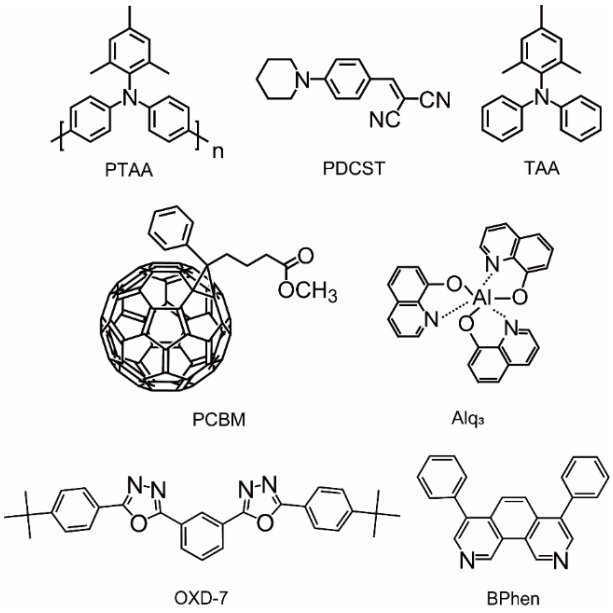

Figure 2.1 Structural formulae of the materials.

2.1.2 Material purification and synthesis

2.1.2.1 Purification of PTAA

PTAA was used after reprecipitation with chloroform (as a good solvent) and hexane (as a poor solvent). The precipitate was collected by the centrifugation method (4000 rpm, 20 min) to yield pale yellow powder of PTAA (95.1% yield, M_w: 22,000 g mol^{-1}, M_w/M_n: 1.8, T_g: 60.7 °C).

2.1.2.2 Synthesis of piperidinodicyanostyrene (PDCST)

A solution of 4-fluorobenzaldehyde (26.2 g, 0.21 mol), azepane (19.7 g, 0.23 mol) and K_2CO_3 (32.0 g, 0.23 mol) in dimethyl sulfoxide (500 mL) was stirred at 50 °C for 20 h under a nitrogen atmosphere. The reaction mixture was diluted with a large amount of water (1 L) and extracted with ethyl acetate (200 mL, 4 times). The combined organic layer was dehydrated by adding anhydrous $MgSO_4$, and the filtered solution was concentrated using an evaporator. The resulting crude product was purified by a column chromatography on silica gel with hexane/ethylacetate (3:1) as an eluent to yield brown solid of 4-piperidinobenzaldehyde (29.0 g, 0.15 mol, 71.4%). R_f 0.4 (for hexane/ ethylacetate 6/1, v/v); ^{1}H NMR (300 MHz, $CDCl_3$, δ): 1.67 (m, 6H; 3,4,5-aze), 4.27 (m, 4H; 2,6-aze), 6.89 (d, 2H, *J* = 9.0; 3,5-Ph), 7.73 (d, 2H, *J* = 9.0; 2,6-Ph), 9.74 (s, 1H; CHO). TOF/MS (ESI, *m/z*): [M Na+] calcd for $C_{12}H_{15}NO$, 189.25; found, 212.1.

4-Dimethylaminopyridine (0.3 g, 2.7 mmol) was added to a solution of 4-piperidinobenzaldehyde (29.04 g, 0.15 mol) and malononitrile (15.2 g, 0.23 mol) in methanol (800 mL) at room temperature, and stirred the mixture for 24 h. The crude product was filtered and recrystallized from ethanol to yield piperidinodicyanostyrene (PDCST) as a yellow plate crystals (31.34 g, 0.13 mol, 62.8%). R_f 0.2 (for hexane/ethylacetate 6/1, v/v); mp 125.7–127.6 °C; ^{1}H NMR (300 MHz, $CDCl_3$, δ): 1.70 (m, 6H; 3,4,5-aze), 3.49 (m, 4H; 2,6-aze), 6.85 (d, 2H, *J* = 9.3; 3,5-Ph), 7.45 (s, 1H; PhCH), 7.78 (d, 2H, *J* = 9.0 Hz; 2,6-Ph). TOF/MS (ESI, *m/z*): [M Na+] calcd for $C_{15}H_{15}N_3$, 237.3; found, 260.1. UV−vis ($CHCl_3$): λ_{max} (ε) = 439 (52900).

2.1.2.3 Synthesis of (2,4,6-trimethylphenyl)diphenylamine (TAA)

A dehydrated toluene (400 mL) solution of diphenylamine (28.3 g, 167 mmol) and sodium *tert*-butoxide (48.2 g, 502 mmol) was added to a solution of tris(dibenzylideneacetone)dipalladium-(0) ($Pd_2(dba)_3$) (0.51 g, 0.55 mmol), and 2-(di-*tert*-butylphosphino)biphenyl (1.0 g, 3.30 mmol) in dehydrated toluene (100 mL) at 0 °C under a nitrogen ambiance. Mesityl bromide (33.3 g, 167 mmol) was added slowly to a mixture with stirring and the mixed solution was kept stirring at 100 °C for 40 h. The reaction mixture was poured into hexane (1000 mL), and the precipitate was removed by the centrifugation method (4000 rpm) a couple of times. Then, the supernatant solution was collected and concentrated using an evaporator. The crude product was purified by a column chromatography with hexane/dichloromethane (2:1) as an eluent and recrystallized from methanol to yield a white solid of (2,4,6-trimethylphenyl)diphenylamine (TAA) (23.0 g, 80 mmol, 48.0%). Rf: 0.4 (for hexane/dichloromethane 3/2, v/v); mp 86.1-89.7 °C; ^{1}H NMR(300 MHz, $CDCl_3$, δ): 2.02 (s, 6H; 2,6-CH_3), 2.33 (s, 3H; 4′-CH_3), 6.92 (t, *J* = 7.5, 2H; 3′,5′-Ph), 6.97 (s, 2H; 3′-Ph), 7.03 (d, *J* = 7.5 Hz, 4H; 2,6-Ph), 7.22 (t, *J* = 7.5 Hz, 8H; 3,5-Ph); TOF/MS (ESI, *m/z*): [M+1] calcd for $C_{21}H_{21}N$, 287.4; found, 284.1. Anal. Calcd for $C_{21}H_{21}N$: C 87.76, H 7.36, N 4.87; found: C 86.95, H 7.23, N 4.84.

2.1.3. Preparation of the SAM modified ITO electrode

Fermi level of indium-tin-oxide (ITO) electrode, -4.8 eV is close to the HOMO (highest occupied molecular orbital) level of PTAA, -5.2 eV, which leads to the large dark current flow at higher electric field. To reduce the dark current flow, ITO electrode was modified with aminopropyltrimethoxysilane (APTMS) to make a self-assembled monolayer (SAM) on an ITO electrode. Fermi level of a SAM modified ITO electrode is -4.3 eV and the dark current of PR device was drastically reduced and the dielectric breakdown of the PR device was suppressed. [1]. The SAM modified ITO electrode was prepared as follows. ITO glass substrates were soaked in solution of H_2O:NH_3:H_2O_2 (5:1:1 by volume) for 15 min to form the hydroxylated ITO surface. Then, hydroxylated ITO electrode was soaked in 1% APTMS in methanol for 30 min to organize APTMS multilayer. Finally, the multilayer was rinsed in 2-propanol, resulting in a SAM modified ITO of APTMS top of ITO electrode.

2.1.4. Composite preparation

The mixture of the PR materials including a photoconductive polymer, NLO dye, plasticizer, and sensitizer was stirred in a tetrahydrofuran (THF) for 24 h, and then cast on a hot plate at 70 °C for 24 h. The resulting polymer composite was sandwiched between two ITO glass plates modified with SAM at 160 ℃ to fabricate a PR composite. The thickness of the PR composite device was controlled using Teflon spacers.

2.2. Measurements

The diffraction efficiency and response time of the PR composites were evaluated using a degenerate four-wave mixing (DFWM) technique as shown in Figure 2.2 [2]. PR gratings were recorded using intersected *s*-polarized laser beams of He-Ne laser or diode-pumped solid-state (DPSS) lasers. The various laser sources used in this study are as follows:

[i] λ = 632.8 nm (He–Ne laser, 10 mW, 0.221 W cm^{-2}, CVI Melles Griot),

[ii] λ = 594 nm (DPSS laser, 25 mW, 0.394 W cm^{-2}, Cobolt Systems, Sweden),

[iii] λ = 561 nm (DPSS laser, 25 mW, 0.265 W cm^{-2}, Cobolt Systems, Sweden),

[iv] λ = 532 nm (DPSS laser, 25 mW, 0.535 W cm^{-2}, Cobolt Systems, Sweden),

[v] λ = 491 nm (DPSS laser, 25 mW, 0.377 W cm^{-2}, Cobolt Systems, Sweden)

The *s*-polarized beams were incident onto the positively biased electrode at an angle of 42.5° (57.5°) for writing beam A (B) relative to the device's normal angle, which corresponds to an internal angle of θ_A = 23.42° (θ_B = 29.74°) according to Snell's law, with an index of refraction n = 1.7. A *p*-polarized reading beam with much weaker intensity from the same source that propagates in the

opposite direction of the writing beam was diffracted by the refractive index gratings in the PR composite. A high voltage amplifier (Trek 610E, USA) or a fast high-voltage amplifier (Trek model 10/10E, USA) were used to supply applied voltage to the PR sample device. The fast high-voltage amplifier was used to supply a rectangular high voltage at 100 Hz to the PR composites. The transmitted and diffracted signals were detected by two photodiode detectors, D1 and D2, respectively.

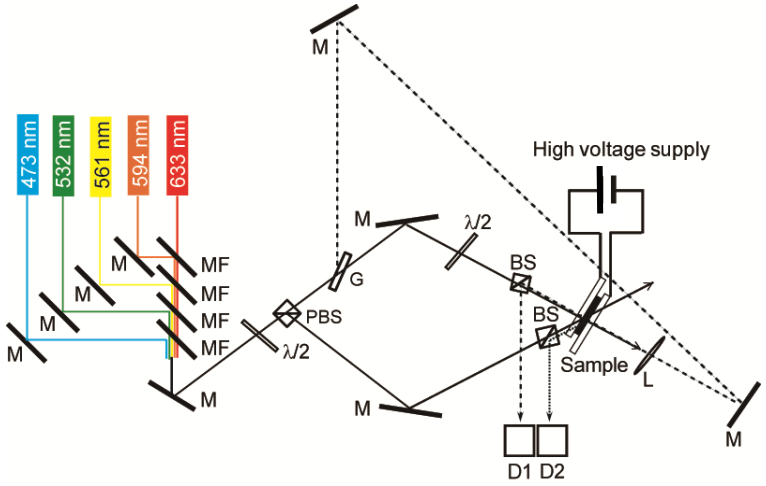

Figure 2.2. Schematic representation of the degenerated four-wave mixing technique with different types of writing lasers: M = mirror, MF = flipper optical mount, L = lens, BS = beam splitter, PBS = polarizing beam splitter, ND = neutral density filter, D = photodiode, $\lambda/2$ = half wave plate.

2.3. Data Analysis

Internal diffraction efficiency (η) was calculated using the intensities of the diffracted beam (I_d) and transmitted beam (I_t) in the equation (2.1):

$$\eta(\%) = \frac{I_d}{I_t + I_d} \times 100 \qquad (2.1)$$

The PR response time (τ) was estimated using a stretched exponential function of Kohlrausch-Williams-Watts (KWW) in the equation (2.2):

$$\eta(\%) = \eta_0 \left\{1 - \exp\left[-\left(\frac{t}{\tau}\right)^{\beta}\right]\right\} \qquad (2.2)$$

where t is the time, η_0 is the steady-state diffraction efficiency, and $\beta\,(0 < \beta \leq 1)$ is a parameter related to the dispersion of the release time from the traps.

The external diffraction efficiency (η_{ext}) was calculated using the equation (2.3):

$$\eta_{\text{ext}} = \exp\left(-\frac{\alpha d}{\cos\theta_{\text{A}}}\right)\eta \tag{2.3}$$

where α is the absorption coefficient, d is the thickness of the sample device and θ_{A} is the internal angle of beam A.

The empirical sensitivity (S) was defined by the equation (2.4):

$$S = \frac{\sqrt{\eta_{\text{ext}}}}{I\tau} \tag{2.4}$$

where I is the intensity of the illuminated laser.

The asymmetric energy transfer was measured using a two-beam coupling (TBC) technique. The laser intensity of two beams crossing through the sample was monitored using photodiodes to measure the optical gain coefficient (Γ) in the equation (2.5):

$$\Gamma = \frac{1}{d}\left[\cos\theta_{\text{A}} \ln\frac{I_1(I_2 \neq 0)}{I_1(I_2 = 0)} - \cos\theta_{\text{B}} \ln\frac{I_2(I_1 \neq 0)}{I_2(I_1 = 0)}\right]. \tag{2.5}$$

where d is the thickness of the sample device; θ_{A} and θ_{B} are the internal angles between the normal to the sample surface and the recording beams A and B, respectively; and I_1 and I_2 are the transmitted intensities of the respective beams.

The PR response time of optical gain (τ_{TBC}) was estimated using a stretched exponential function of Kohlrausch-Williams-Watts (KWW) in the equation (2.6):

$$\Gamma = \Gamma_0\left\{1 - \exp\left[-\left(\frac{t}{\tau}\right)^{\beta}\right]\right\} \tag{2.6}$$

where t is the time, Γ_0 is the steady-state optical gain coefficient, and β ($0 < \beta \leq 1$) is a parameter related to the dispersion of the release time from the traps.

A steady-state photocurrent was recorded using a current monitor equipped in a Trek 610E high-voltage amplifier when the steady-state DFWM signal was measured.

References and links

[1] K. Kinashi, H. Shinkai, W. Sakai and N. Tsutsumi, "Photorefractive device using self-assembled monolayer coated indium-tin-oxide electrodes," *Org. Electron.* **14**(11), 2987–2993 (2013).

[2] K. Kinashi, Y. Wang, W. Sakai, and N. Tsutsumi, "Optimization of photorefractivity based on poly(Nvinylcarbazole) composites: An approach from the perspectives of chemistry and physics," *Macromol. Chem. Phys.* **214**(16), 1789–1797 (2013).

Chapter 3: Photorefractive performance of poly(triarylamine)-based polymer composites

3.1. Introduction

PR materials are the promising media for providing updatable or rewritable holographic 3D imaging [1]. Faster response is preferred for the dynamic photorefractive applications. All optical dynamic correction of distorted image was demonstrated using PR device [2]. In this research, the amorphous methyl-substituted main-chain type poly(triarylamine) (PTAA) with a high hole mobility (10^{-2} cm^2 V^{-1} s^{-1}), used in the organic field effect transistors [3, 4], was chosen as a photoconductive polymer and adapted to PR polymer composites. PR performances of internal diffraction efficiency from 4 to 6 % and a response time of 11.3 ms were reported using the PTAA-based PR composites [5]. The obtained response time of 11.3 ms satisfies the criterion for the video-rate quality (30 ms), but the diffraction efficiency is too low for the holographic applications. Main reason for the low diffraction efficiency is ascribed to the large photocurrent, because it limits the applied electric field up to 20 $V\mu m^{-1}$. Namely large photocurrent in the PTAA PR composites induced easy dielectric breakdown at the electric field higher than 25 $V\mu m^{-1}$. Thus, each component in the PTAA PR composites should be redesigned to control the photocurrent, which guarantees the high performance PR devices. In this thesis, we redesign each component of the PTAA-based PR composites to achieve the best PR performances.

In chapter 3, the PR performance of the PTAA-based PR composite was improved by optimizing the content of sensitizer. The PR characteristics of diffraction efficiency up to 78% and faster response time close to 5 ms were achieved.

3.2. Experimental

The detailed description about the materials and sample preparation were explained in section 2.1 in chapter 2. PTAA as photoconductive polymer, PDCST as a NLO dye, TAA as a plasticizer, and PCBM as a sensitizer were used in this chapter (Fig.3.1). The compositions of PDCST and TAA were fixed at 35 and 20 by weight, respectively, and the composition ratio between PTAA and PCBM were changed to 42/3, 44/1, 44.5/0.5, 44.7/0.3, 44.9/0.1, and 45/0 by weight. The THF solution of PTAA, PDCST, TAA, and PCBM were stirred for 24 h, and then cast on a hot plate at 70 °C for 24 h. The resulting PR composite was sandwiched between two SAM-modified ITO glass plates at 160 °C to fabricate a PR composites. The thickness of the PR composite was controlled to 50 μm using Teflon spacers.

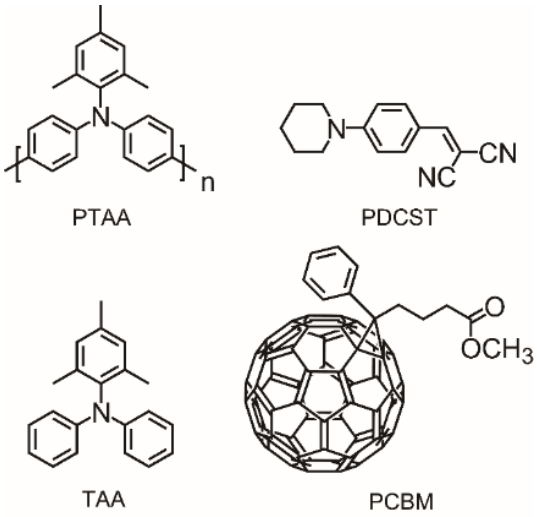

Fig. 3.1. Structural formulae of PR materials used in this chapter.

3.3. Measurements

The UV–Vis absorption spectrum of each PR composite was measured using a Perkin–Elmer Lambda 1050 UV/Vis/NIR spectrophotometer. The absorption coefficient a is given by $\alpha = A\ln(10)/d$, where A is the measured absorbance and d is the thickness of the PR composite.

The diffraction efficiency η and the response time τ of the PR composites was measured using a degenerate four-wave mixing (DFWM) technique [6]. The various laser sources are used: a He–Ne laser with $\lambda = 632.8$ nm (10 mW) and the diode-pumped solid-state (DPSS) lasers with $\lambda = 594$ nm (25 mW), $\lambda = 561$ nm (25 mW), $\lambda = 532$ nm (25 mW), and $\lambda = 491$ nm (25 mW).

Asymmetric energy transfer in the PR composite was measured using a two-beam coupling (TBC) technique. The intensities of the two beams transmitted through the PR composite were monitored with photodiode detectors to measure the optical gain coefficient Γ [7]. Then, response time τ_{TBC} was calculated.

Empirical sensitivity S is defined by $\eta_{ext}^{1/2} / I\tau$, where η_{ext} is the external diffraction efficiency at an exposure time, τ is the response time, and I is the intensity of the illuminated laser [6].

3.4. Results and Discussion

3.4.1. Optimizing the content of PCBM

To optimize the content of PCBM, the diffraction efficiency, the response time, and the sensitivity were measured as a function of PCBM content in the PR composite under an applied field of 45 V μm^{-1} at 632.8 nm. The composition of PTAA/PDCST/TAA/PCBM is 45-*X*/35/20/*X* by wt., where *X* is ranged from 0 to 3 wt%. The PR parameters are plotted in Figure 3.2. At a PCBM content of 0.5 wt%, a maximum sensitivity of 43 cm^2 J^{-1} is measured with response time of 5 ms and a diffraction efficiency of 16.6% at 632.8 nm with the beam intensity of 1.5 W cm^{-2}. Therefore, PTAA/PDCST/TAA/PCBM (44.5/35/20/0.5 by wt.) was determined as an appropriate composition in this chapter.

Figure 3.3 shows a plot of the diffraction efficiency as a function of the applied field for the PTAA-based PR composite (PTAA/PDCST/TAA/PCBM, 44.5/35/20/0.5 by wt.). The resulted diffraction efficiency is significantly increased with increasing the applied field until it reaches a maximum diffraction efficiency of 49.7 ± 13.7% under an applied field of E = 85 V μm^{-1} and at 632.8 nm with the beam intensity of 0.067 W cm^{-2}; the beam intensity is extremely lowered to avoid the dielectric breakdown under a high applied electric field. The diffraction signals are lowered at larger fields greater than 90 V μm^{-1}, due to the over modulation of the refractive index. Large error bars of the diffraction at higher applied field range of 70 – 110 V μm^{-1} are measured. Therefore, lower region on the electric field is favorable. Thus, applied field of 45-60 V μm^{-1} are chosen for the following measurements.

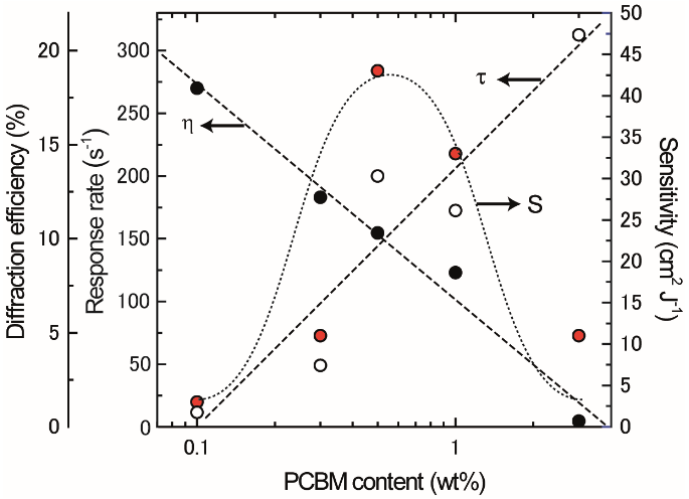

Fig. 3.2. Plots of diffraction efficiency η (black circle), inverse response time τ^{-1} (white circle), and sensitivity S (red circle) as a function of PCBM content under an applied field of 45 V μm^{-1} and 632.8 nm illumination (I = 1.5 W cm^{-2}).

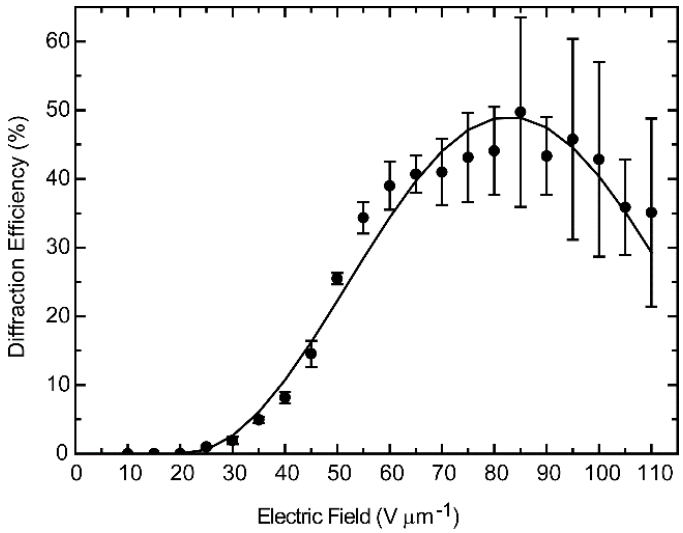

Fig. 3.3 Diffraction efficiency as a function of applied field at 632.8 nm light (I = 0.067 W cm^{-2}).

3.4.2. Wavelength dependence of the PTAA-based PR composite

Figure 3.4 shows the wavelength dependence on diffraction efficiency as a function of time for the composite (PTAA/PDCST/TAA/PCBM, 44.5/35/20/0.5 by wt.) under an applied field of 45 V μm^{-1}. The optical diffraction performance at 491 nm illumination was monitored using 632.8 nm He-Ne laser as a probe beam because of the strong absorption (high absorption coefficient) of PR device at 491 nm. The obtained PR quantities are summarized in Table 3.1. The maximum diffraction efficiency and the fastest response time are measured at 532 nm. At longer wavelengths, 561, 594, 632.8 nm and shorter wavelength 491 nm, diffraction efficiency is lower and response time is slower.

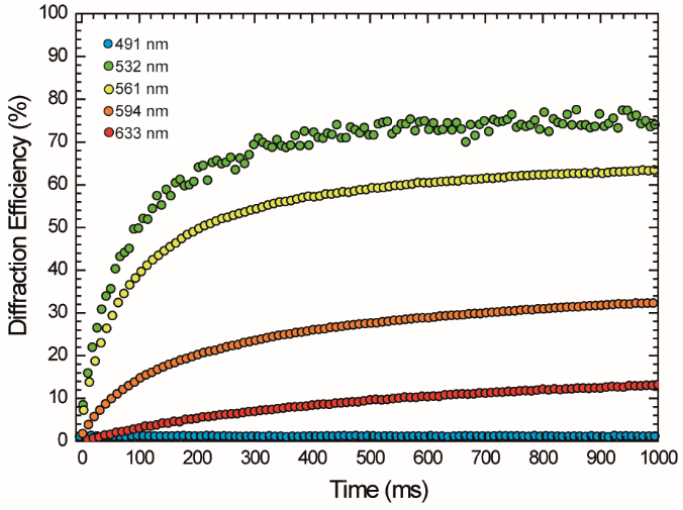

Figure 3.4. Wavelength dependence on diffraction efficiency as a function of time under an applied field of 45 V μm^{-1}.

Table 3.1. PR quantities and parameters for various laser wavelengths. Applied field: 45 Vμm^{-1}.

λ (nm)	I_0 (W cm^{-2})	α (cm^{-1})	η (η_{ext}) (%)	Δn (10^{-3})	Γ (cm^{-1})	τ (ms) / β	S (cm^2 J^{-1})
491[1)]	0.377	968	0.2 (0.1[2)])	n/a	n/a	3164 / 0.98	0.1
532	0.0976	384	78.2 (2.6)	2.01	128.0	107 / 0.61	15
561	0.0520	174	64.6 (13.8)	1.82	143.8	135 / 0.64	53
594	0.0712	85	42.5 (13.8)	1.47	100.4	532 / 0.52	12
632.8	0.0670	48	42.6 (27.9)	1.57	87.1	766 / 0.53	10

[1)]Probed by 632.8 nm. [2)]Calculated using the absorption coefficient at 632.8 nm.

Although the maximum diffraction efficiency and the fastest response time are evaluated at 532 nm illumination, the highest sensitivity is calculated at 561 nm. The sensitivity at 532 nm was lower due to higher absorption coefficient, resulting in low external diffraction efficiency. Here one issue is arising; how we design the composition of the PR composite to control the absorption coefficient smaller to achieve simultaneously higher external diffraction efficiencies and faster response time. Lower absorption coefficient is also merit for the multi-color or full-color holographic display applications. Improvement of the external diffraction efficiency for PTAA-based PR composite is described in the chapter 5.

3.4.3. Writing beam intensity dependence of PR quantities

Generally, the intensity of the writing beam significantly affects the response times for the optical diffraction and the optical gain. Figure 5.3 shows a plot of the response times for optical diffraction, τ and those of optical gain, τ_{TBC} as a function of the writing beam intensity at 532 nm (a) and 632.8 nm (b) for the PTAA-based PR composite (PTAA/PDCST/TAA/PCBM, 44.5/35/20/0.5 by wt.). The obtained PR quantities are summarized in Table 3.2.

Dynamic PR performance is strongly affected by the writing beam intensity: the τ value for the optical diffraction become faster with increasing the intensity of the laser beam at both wavelengths; the value of τ_{TBC} for the optical gain due to the asymmetric energy transfer also become faster with increasing the laser intensity except for the case of optical gain measurement under the illumination at 632.8 nm with the beam intensity of 0.0278 W cm^{-2}. Comparing each τ_{TBC} value and corresponding τ value, the τ_{TBC} value is faster than the τ value except for the case of 532 nm illumination with the beam intensity of 0.427 W cm^{-2}. The τ_{TBC} value is 5–10 times faster than the τ value. In many cases, the TBC gain builds up faster than the diffraction signal [8].

(a) 532 nm (b) 632.8 nm

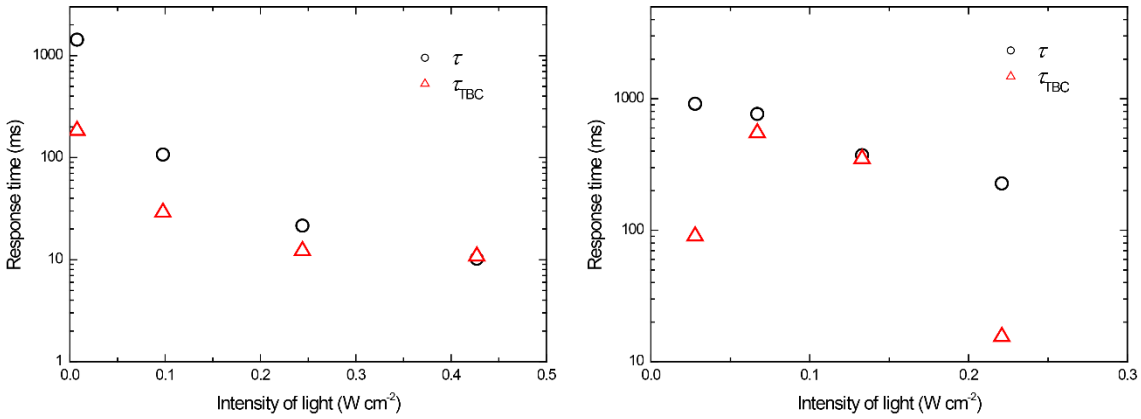

Figure 3.5. Plots of response time as a function of writing beam intensity at 532 nm (a) and 632.8 nm (b) under an applied field of 45 V μm^{-1}.

Table 3.2. PR quantities and parameters for various intensities at 532 nm (a) and 632.8 nm (b). Applied field: 45 Vμm^{-1}.

(a) 532 nm

I_0 (W cm^{-2})	η (η_{ext}) (%)	Δn (10^{-3})	Γ (cm^{-1})	Δn_{TBC} (10^{-4})	τ (ms) / β	τ_{TBC} (ms) / β	S (cm^2 J^{-1})
0.427	47.0 (1.6)	1.40	148.3	6.28	10.2 / 0.75	10.8 / 0.99	29
0.244	47.3 (1.6)	1.40	143.7	6.08	21.5 / 0.60	12.2 / 0.96	24
0.0976	78.2 (2.6)	2.01	128.0	5.48	107 / 0.61	29.1 / 0.86	15
0.00748	29.4 (0.97)	1.06	151.7	6.42	1427 / 0.86	184 / 1.0	9

(b) 632.8 nm

I_0 (W cm^{-2})	η (η_{ext}) (%)	Δn (10^{-3})	Γ (cm^{-1})	Δn_{TBC} (10^{-4})	τ (ms) / β	τ_{TBC} (ms) / β	S (cm^2 J^{-1})
0.221	46.2 (30.3)	1.64	62.2	3.13	227 / 0.53	15.5 / 0.53	11
0.133	46.8 (30.7)	1.66	109.5	5.52	372 / 0.59	350 / 0.98	11
0.0670	42.6 (27.9)	1.54	87.1	4.39	766 / 0.53	550 / 0.71	10
0.0278	36.4 (23.9)	1.42	82.2	4.14	915 / 0.69	90.4 / 0.76	19

3.6 Conclusions

The PR performance of the PTAA-based PR composite was enhanced via changing the ratio of PCBM. The PTAA-based PR with the composition of PTAA/PDCST/TAA/PCBM (44.5/35/20/0.5 by wt.) showed the PR characteristics of the diffraction efficiency of 16.6%, the response time of 5.0 ms, and the sensitivity of 43 $cm^2\ J^{-1}$ at 632.8 nm (1.5 W cm^{-2}) under an applied field of 45 V μm^{-1}.

Wavelength dependency of the PR performance was examined. The shorter wavelength induced higher diffraction efficiency and faster response time due to the appropriate charge generation.

The TBC gain builds up faster than the optical diffraction signal. The response times for the optical diffraction and the optical gain were faster with increasing recording laser intensity. A response time of 10.2 ms with a diffraction efficiency of 47.0% was obtained under an applied field of 45 V μm^{-1} and 532 nm illumination with a beam intensity of 0.427 W cm^{-2}.

References and links

[1] S. Tay, P. A. Blanche, R. Voorakaranam, A. V. Tunc, W. Lin, S. Rokutanda, T. Gu, D. Flores, P. Wang, G. Li, P. St Hilaire, J. Thomas, R. A. Norwood, M. Yamamoto and N. Peyghambarian, "An updateable 3D holographic display," *Nature* **451**, 694–698 (2008).

[2] G. Li, M. Eralp, J. Thomas, S. Tay, A. Schülzgen, R. A. Norwood and N. Peyghambarian, "All-optical dynamic correction of distorted communication signals using a photorefractive polymeric hologram," *Appl. Phys. Lett.* **86**, 161103–161105 (2005).

[3] P. A. Bobbert, A. Sharma, S. G. J. Mathijssen, M. Kemerink and D. M. de Leeuw, "Operational stability of organic field-effect transistors," *Adv. Mater.* **24**(9), 1146–1158 (2012).

[4] J. Smith, W. Zhang, R. Sougrat, K. Zhao, R. Li, D. Cha, A. Amassian, M. Heeney, I. McCulloch and T. D. Anthopoulos, "Solution-processed small molecule-polymer blend organic thin-film transistors with hole mobility greater than 5 cm^2/Vs," *Adv. Mater.* **24**(18), 2441–2446 (2012).

[5] K. Kinashi, H. Shinkai, W. Sakai and N. Tsutsumi, "Photorefractive device using self-assembled monolayer coated indium-tin-oxide electrodes," *Org. Electron.* **14**(11), 2987–2993 (2013).

[6] K. Kinashi, Y. Wang, W. Sakai and N. Tsutsumi, "Optimization of photorefractivity based on poly(*N*-vinylcarbazole) composites: An approach from the perspectives of chemistry and physics," *Macromol. Chem. Phys.* **214**(16), 1789–1797 (2013).

[7] P. Günter and J. P. Huignard, "Photorefractive Materials and Their Applications II," *Springer-Verlag* (1988).

[8] S. Köber, F. Gallego-Gomez, M. Salvador, F. B. Kooistra, J. C. Hummelen, K. Aleman, S. Mansurovac and K. Meerholz, "Influence of the sensitizer reduction potential on the sensitivity of photorefractive polymer composites," *J. Mater. Chem.*, **20**(29), 6170–6175 (2010).

Chapter 4: Photorefractive response and photocurrent of poly(triarylamine)-based polymer composite with second electron trap

4.1. Introduction

In chapter 3, a response time of 10.2 ms and a diffraction efficiency of 47.0% were observed for PTAA/PDCST/TAA/PCBM (44.5/35/20/0.5 by wt.) under an applied field of 45 V μm^{-1} and 532 nm illumination with an intensity of 0.427 W cm^{-2}. The beam intensity was weakened to avoid the dielectric breakdown in a small applied field. The dielectric breakdown arose from the high photocurrent of the PTAA-based PR composite. A drastic improvement in the PR response was reported by adding a second electron acceptor, tris(8-hydroxyquinolinato)aluminium (Alq_3), which acted as another trapping sites for electrons and suppressed dielectric breakdown [1].

In this chapter, the PR response and dynamics of a PTAA-based PR polymer composite with small amount of a second electron acceptor were investigated. Alq_3, 1,3-Bis[2-(4-*tert*-butylphenyl)-1,3,4-oxadiazo-5-yl]benzene (OXD-7) and bathophenanthroline (BPhen) were used as second electron trap agents in the PTAA-based PR composite. Using BPhen and Alq_3 as the second electron trap leaded to sub-millisecond response time suppressing photocurrent. The effect of photoconductivity on the PR response time was also discussed.

4.2. Experimental

The detailed description about the materials and sample preparation were explained in section 2.1 in chapter 2. PTAA as photoconductive polymer, PDCST as a NLO dye, TAA as a plasticizer and PCBM as a sensitizer were used in this chapter. As a second electron acceptor, Alq_3, OXD-7 or BPhen were introduced to the PTAA-based PR composite. The structural formulae of materials are listed in Fig. 4.1. The composition ratio of PDCST, TAA and PCBM was fixed at 35, 20, and 0.5 by weight, respectively. The ratio of PTAA and each second electron trap were changed to 43.5/1 and 44.5/0 (as a reference) by weight. The THF solution of each mixture of the materials were stirred for 24 h and then cast on a hot plate at 70°C for 24 h. The resultant composites were sandwiched between two ITO electrodes modified with a SAM of APTMS on hot plate at 160 °C. The film thickness of each PR composite was adjusted to 50 μm with using Teflon spacers.

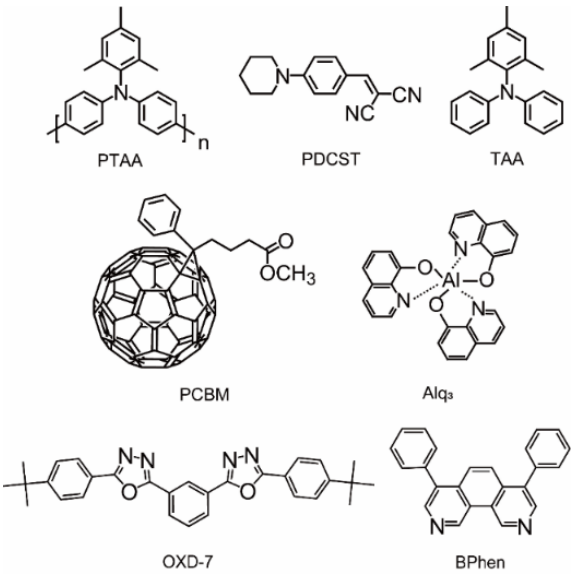

Fig. 4.1 Structural formulae of PR materials used in this chapter.

4.3. Measurements

The UV-Vis spectra of PR composites were measured using a Lambda1050 UV/Vis/NIR spectrophotometer (Perkin-Elmer Co., USA). The absorption coefficient α was calculated by $\alpha = A\ln(10)/d$, where A is the absorbance and d is the film thickness of the PR sample. The film thickness was adjusted to 20 - 30 μm so as not to exceed an A of 1 in the short wavelength region.

The diffraction efficiency η and the response time τ of the PR composites was measured using a degenerate four-wave mixing (DFWM) technique. PR gratings were written in the PR device by the intersected *s*-polarized beams of a diode-pumped solid-state (DPSS) laser with λ = 532 nm (25 mW, 0.534 W cm^{-2}, Cobolt AB, Sweden). A rectangular high voltage with a 100 Hz frequency was applied to the PR device using a high-voltage amplifier (Trek 10/10E, USA). As a comparison of applying a rectangular voltage, a sequence response of the optical diffraction when the laser light is chopped with using an optical chopper at 99 Hz under applied electric field.

Asymmetric energy transfer in the PR composite was measured using a two-beam coupling (TBC) technique. The intensities of the two beams transmitted through the PR composite were measured with photodiode detectors to evaluate the optical gain coefficient Γ. Photocurrent was monitored using a Trek 610E high voltage amplifier when the DFWM signal was recorded.

Empirical sensitivity S is estimated by $\eta_{ext}^{1/2} / I\tau$, where η_{ext} is the external diffraction efficiency at an exposure time, τ is the response time, and I is the intensity of the light.

4.4. Results and Discussion

4.4.1. Effect of second electron traps

In chapter 3, a response time of 10.2 ms and a diffraction efficiency of 47.0% were measured for PTAA/PDCST/TAA/PCBM (44.5/35/20/0.5 by wt.) under an applied field of 45 V μm^{-1} and 532 nm illumination with an intensity of 0.427 W cm^{-2}. For further PR performance of the PTAA-based composite, higher applied field operation with higher intensity of light were required. In this chapter, the light intensity was fixed to 0.534 W cm^{-2} for the maximum operation of the laser source.

The photocurrent is plotted as a function of the electric field for the PTAA-based PR composites in Fig. 4.2. Without a second electron trap (blank in Fig. 4.2), the photocurrent over 100 μA was measured and a dielectric breakdown was occurred at the electric field above 40 V μm^{-1} for the PTAA-based composite. Furthermore, without a second electron trap the higher intensity of 0.534 W cm^{-2} leads to the dielectric breakdown in the lower electric field. On the other hands, the photocurrents are reduced over the entire electric field for the composites with the second electron traps, almost leveling off at an electric field above 40 V μm^{-1}, which reduces the risk of dielectric breakdown at high electric fields up to 60 V μm^{-1}. The addition of BPhen reduces the photocurrent by 53 μA at 60 V μm^{-1}.

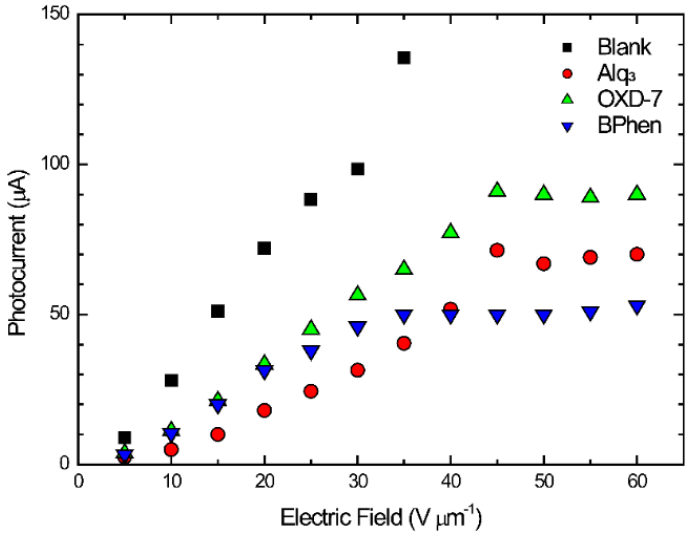

Fig. 4.2. Photocurrent as a function of the applied field for PR composites with second electron traps.

The UV-Vis spectra of the PTAA-based composites are shown in Fig. 4.3. Compared with the spectrum for the blank, the addition of Alq_3 and BPhen exhibits the broad absorption spectra with a peak at approximately 560 nm, attributing to the charge-transfer (CT) complex between PTAA and Alq_3 or BPhen. The degree of the CT complex of BPhen is higher than that of Alq_3. On the other hand, the addition of OXD-7 leads to a decrease in the absorption coefficient and no CT complex.

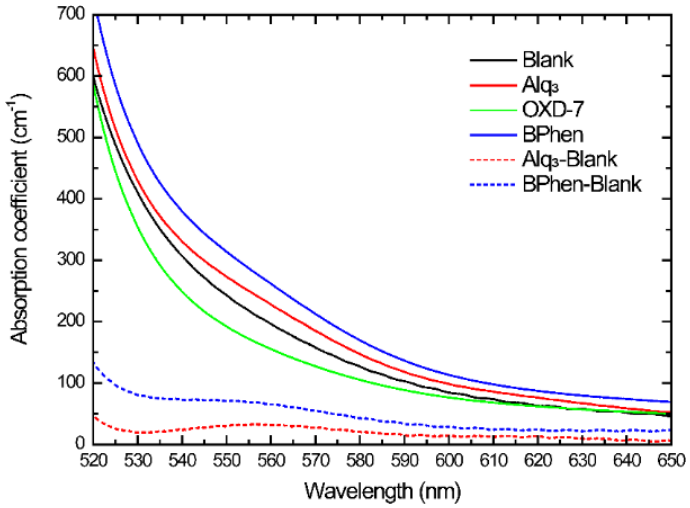

Fig. 4.3. UV-Vis spectra of PTAA-based PR composites with second electron traps. The dashed curves are the spectra due to charge transfer between PTAA and the second electron trap.

Here, HOMO and LUMO levels are listed for three electron traps and PTAA [2] in Table 1. The LUMO level of PTAA was estimated from the HOMO level and absorption edge of PTAA. There are not much differences in HOMO and LUMO levels between three electron acceptors. In this case, the ability of the CT complex formation is significantly related to the reduction of photocurrent.

Figure 4.4 and 4.5 show the energy level diagram of the HOMO-LUMO levels for the PTAA-based PR composites with Alq_3 and BPhen, respectively [3, 4]. The absorption of the photon energy by PCBM competes with that by the CT complex between PTAA and electron trap of Alq_3 or BPhen, and therefore the photocurrent resulting from the photoexcitation of PCBM is significantly reduced.

Table 4.1. HOMO and LUMO levels for three electron traps and PTAA.

	Alq3	OXD-7	BPhen	PTAA
LUMO (eV)	-3.3	-3.0	-3.0	-2.2
HOMO (eV)	-6.0	-6.5	-6.4	-5.2

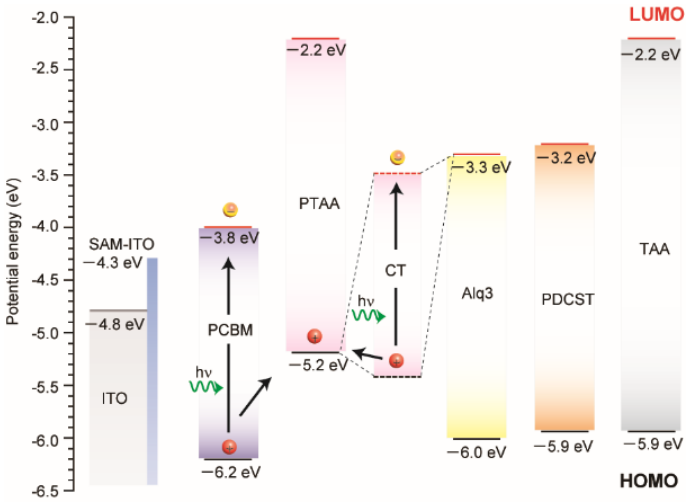

Fig. 4.4. Energy level diagram of the PTAA-based PR composite containing Alq_3.

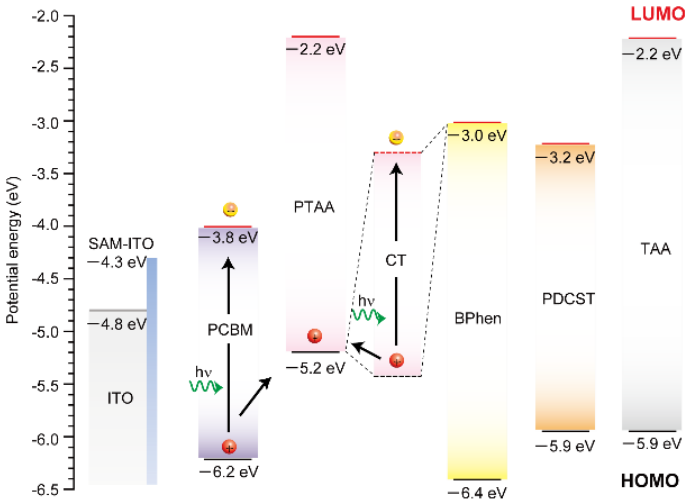

Fig. 4.5. Energy level diagram of the PTAA-based PR composite containing BPhen.

4.4.2. Photorefractive response under a rectangular illumination or a rectangular applied field

In this section, the photorefractive dynamics of the optical diffraction for the PTAA-based PR polymer composite of PTAA/PDCST/TAA/PCBM/Alq_3 (43.5/35/20/0.5/1 by wt.) is investigated using either a rectangular laser illumination or a rectangular applied electric field.

Fig. 4.6 shows the sequence response of the optical diffraction when the laser light is chopped with using an optical chopper at 99 Hz under applied electric field of 60 Vμm^{-1}. The rise of diffraction efficiency and decay correspond to the switching on and off the illumination. The PR composition of PTAA/PDCST/TAA/PCBM/Alq_3 (43.5/35/20/0.5/1 by wt.) shows the PR characteristics of diffraction efficiency of 63.2% and its response time of 1.1 ms and the decay time of 0.83 ms. It is suggested that the addition of Alq_3 leads to the improvement in PR characteristics.

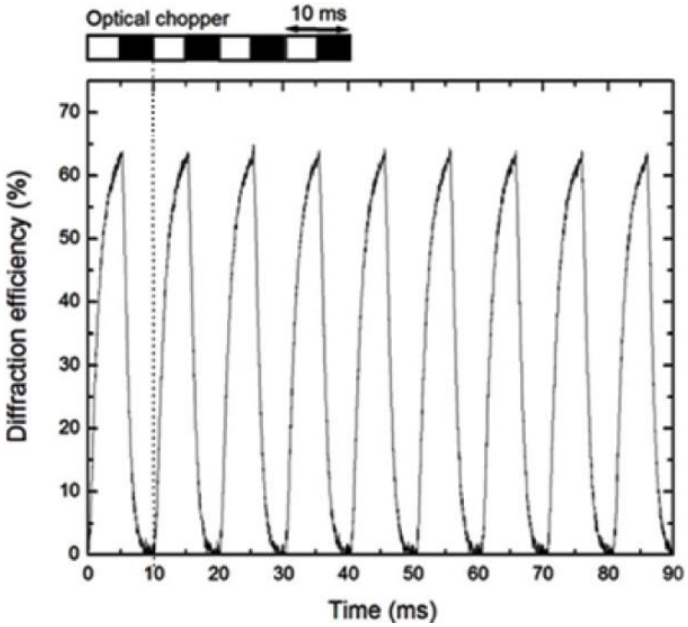

Fig. 4.6. Sequence response of the diffraction efficiency for a PR device with the composition PTAA/ PDCST/TAA/PCBM/Alq3 (43.5/35/20/0.5/1 wt%) with a chopping frequency of 99 Hz. Applied electric field is 60 V μm^{-1}.

Next the sequence response is measured for the optical diffraction when a continuous rectangular field with a frequency of 100 Hz (from 0 V μm^{-1} to 60 V μm^{-1}) is applied to the PR composites. The diffraction efficiency is plotted as a function of time for PTAA/PDCST/TAA/PCBM/ Alq_3 (43.5/35/20/0.5/1 by wt.) in Fig. 4.7. The rise of the diffraction efficiency and the decay correspond to the switching on and off the applied rectangular field. The diffraction efficiency was calculated to be 83.0% with the response time of 860 μs and the decay time of 105 μs.

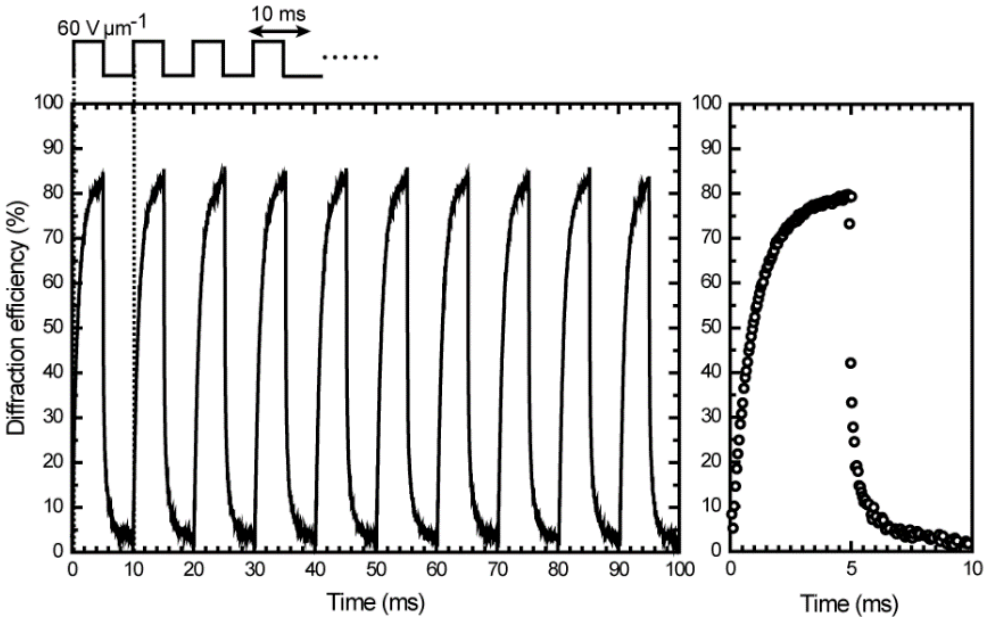

Fig. 4.7. Left: sequence response of the optical diffraction for the composition of PTAA/PDCST/TAA/ PCBM/Alq_3 (43.5/35/20/0.5/1) under a rectangular applied field at a frequency of 100 Hz (from 0 to 60 V μm^{-1}). Right: one cycle response.

Comparing with the difference of the response time between laser beam on/off with constant field in Fig. 4.6 and applied field on/off with constant laser illumination in Fig. 4.7, the latter response time, 860 μs is 30 % faster than the former response time, 1.1 ms. This means the constant laser illumination gives the environment for the faster formation speed of space-charge field when applied electric field is turn on. However, turning off the applied field straightly gives the disappearance of space charge field. The resulting latter decay time, 105 μs is very short, which is almost one eighth of 830 μs for the former decay time.

4.4.3. Photorefractive dynamics with second electron traps

As second electron traps, OXD-7 and BPhen were also investigated. The diffraction efficiency is plotted as a function of time for PTAA/PDCST/TAA/PCBM/ OXD-7 (43.5/35/20/0.5/1 by wt.) in Fig. 4.8. The diffraction efficiency was calculated to be 62.6% with a response time of 997 μs (β = 0.77) and a decay time of 213 μs (β = 0.81).

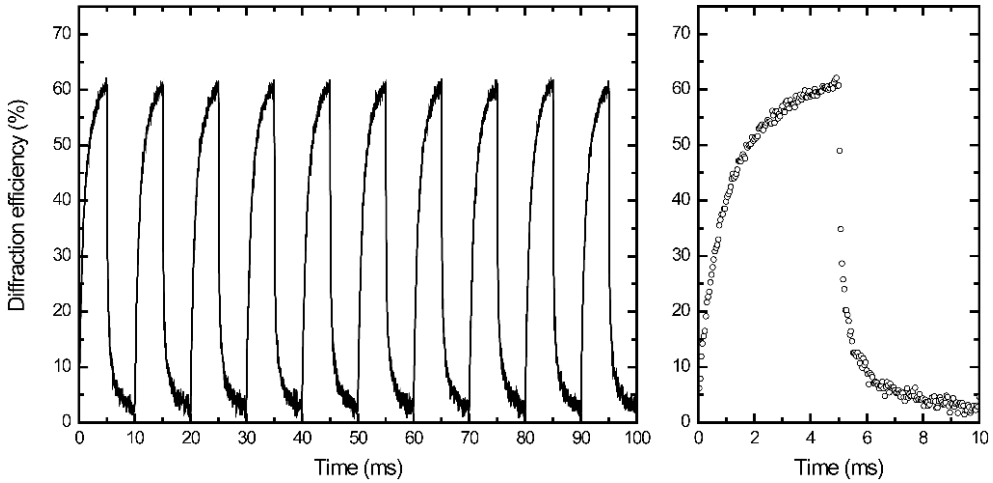

Fig. 4.8. Left: sequence response of the optical diffraction for the composition of PTAA/PDCST/TAA/ PCBM/OXD-7 (43.5/35/20/0.5/1) under a rectangular applied field at a frequency of 100 Hz (from 0 to 60 V μm^{-1}). Right: one cycle response.

The diffraction efficiency of PTAA/PDCST/TAA/PCBM/BPhen (43.5/35/20/0.5/1 by wt.) is plotted as a function of time in Fig. 4.9. The diffraction efficiency was calculated to be 73.3% with a response time τ of 397 μs (β = 0.54) and a decay time τ_d of 1294 μs (β = 0.85). The fast response time of 397 μs is measured for the PR polymer composites. The decay time is three times longer than the response time. It's quite a different from the others: Alq_3 and OXD-7, whose decay time is faster than the response time. This phenomenon is caused by the overmodulation of the refractive index. The diffraction efficiency reached a maximum within 2 ms. Then, the diffraction light decreased from 75% to 69% until the applied field was turned off. Upon turning off the applied electric field, a quick and sharp increase in the diffraction efficiency was measured, indicating the recovery of the diffraction efficiency, which assists the slow dissipation of the diffraction efficiency. The resulting PR parameters were listed in Table. 4.2.

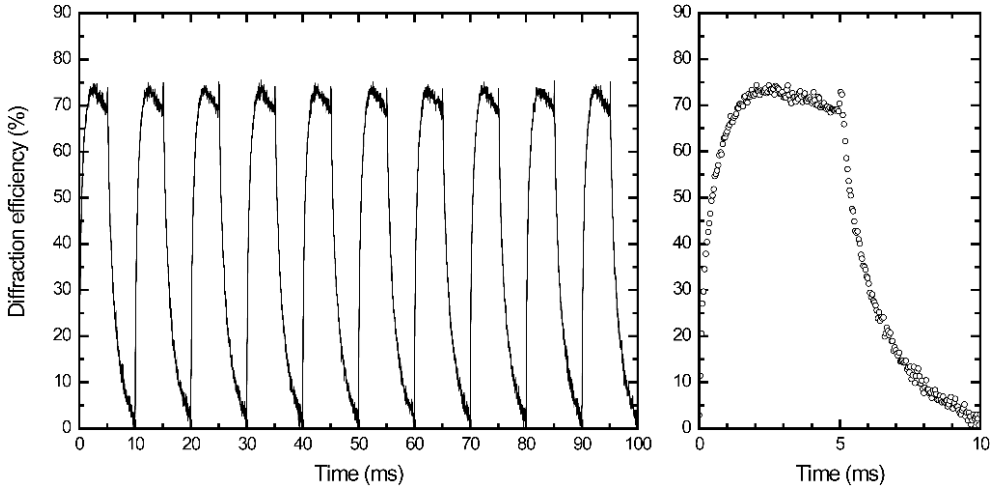

Fig. 4.9. Left: sequence response of the optical diffraction for the composition of PTAA/PDCST/TAA/ PCBM/BPhen (43.5/35/20/0.5/1) under a rectangular applied field at a frequency of 100 Hz (from 0 to 60 V μm^{-1}). Right: one cycle response.

Table 4.2. PR quantities and parameters in the PTAA-based PR composites with second electron traps and without second electron traps (blank).

	α (cm^{-1})	Δn	Γ (cm^{-1})	η (η_{ext}) (%)	τ (μs) / β	τ_d (μs) / β	S (cm^2 J^{-1})
Alq_3	404	3.49×10^{-3}	136.7	83.0 (9.2)	860 / 0.86	105 / 0.45	667
OXD-7	327	2.78×10^{-3}	127.3	62.6 (10.6)	997 / 0.77	213 / 0.81	607
BPhen	462	3.13×10^{-3}	156.4	73.3 (5.9)	397 / 0.54	1294 / 0.85	1145
Blank	384			—*			

*Dielectric breakdown below 40 V μm^{-1}

The sensitivity S including both factors of the diffraction efficiency and the response time is an indicator of the performance of real-time 3D holographic displays. The PTAA-based PR composite with BPhen was estimated to have a sensitivity of 1145 cm^2 J^{-1}, which is almost two times higher than that of the other composites. This extremely high sensitivity is promising for obtaining high-performance PR devices as real-time 3D holographic displays.

As shown in Fig. 4.2, the addition of BPhen significantly reduced the photocurrent at 60 V μm^{-1}, which is due to the reduction of photoexcitation of PCBM by the formation of CT complex between PTAA and BPhen. In the next section, the effect of photocurrent on the response time was discussed.

4.4.4. Photorefractive response and photocurrent

The photoconductive properties related to the photocurrent in the PTAA-based PR composites with second electron traps listed in Table 4.3 were calculated.

The internal photocurrent efficiency $\varphi_{\mathrm{ph}}(E)$ is related to the photocurrent per unit area J_{ph} by the equation (4.1) [5, 6]:

$$\varphi_{\mathrm{ph}}(E) = \frac{J_{\mathrm{ph}} h\nu}{eI_0 \alpha L} = \frac{\sigma_{\mathrm{ph}} E_0 h\nu}{eI_0 \alpha L} \tag{4.1}$$

where σ_{ph} is the photoconductivity, E_0 is the applied field, h is Planck's constant, ν is the light frequency, e is the elemental charge constant, I_0 is the light intensity, α is the absorption coefficient, and L is the thickness of the composite film. $\varphi_{\mathrm{ph}}(E)$ follows the increase of the photocurrent and increased in the order of BPhen < Alq_3 < OXD-7.

The internal photocurrent efficiency $\varphi_{\mathrm{ph}}(E)$ is related to the photocarrier charge generation efficiency η_{p} by the equation (4.2) [6]:

$$\varphi_{\mathrm{ph}}(E) = G\eta_{\mathrm{p}} = \frac{\varepsilon_{\mathrm{r}} \varepsilon_0 E_0 \eta_{\mathrm{p}}}{eLT_{\mathrm{i}}} \tag{4.2}$$

where G is the photoconductivity gain factor and T_{i} is the initial trap density in Schildkraut's model [7]. A dielectric constant ε_{r} of 3.5 was determined through capacitance measurements employing a charge amplifier.

From the aspect of the photocurrent efficiency, $\varphi_{\mathrm{ph}}(E)$ in the equation (4.2), the effect of the second electron trap on the values of η_{p} and T_{i} can be estimated. In the equation (4.2), $\varphi_{\mathrm{ph}}(E)$ is proportional to the ratio of $\eta_{\mathrm{p}}/T_{\mathrm{i}}$. As listed in Table 4.3, $\varphi_{\mathrm{ph}}(E)$ increases in the order of BPhen < Alq_3 < OXD-7, which follows the increase of the response time. Namely, smaller $\varphi_{\mathrm{ph}}(E)$ or $\eta_{\mathrm{p}}/T_{\mathrm{i}}$ leads to the faster response time. Thus, for BPhen samples, smaller η_{p} or larger T_{i} is reasonably evaluated. Smaller η_{p} is ascribed to lower efficiency of photocarrier generation via CT complex between PTAA and BPhen.

The η_{p} values and the T_{i} values were estimated on the following assumption. First, the photocarrier generation efficiency η_{p} is proportional to the photocurrent and never exceeds a unity. Second, the trap density T_{i} is not affected by the applied electric field. Under these assumptions, the appropriate η_{p} values and T_{i} values were calculated and listed in Table 4.3.

The trap-limited space-charge field E_{q} is evaluated by the equation (4.3) [6]:

$$E_{\mathrm{q}} = \frac{eT_{\mathrm{i}}}{\varepsilon_{\mathrm{r}} \varepsilon_0 K_{\mathrm{G}}} \tag{4.3}$$

where K_{G} is the grating vector ($K_{\mathrm{G}} = 2\pi/\Lambda$) and Λ is the grating period.

The Kukhtarev model predicts the space-charge field E_{SC} [8]:

$$E_{SC} = E_q \left(\frac{E_D^2 + E_p^2}{E_p^2 + (E_q + E_D)^2} \right)^{1/2} \tag{4.4}$$

with E_q, the diffusion field E_D ($E_D = K_G kT/e$, where k is Boltzmann's constant, and T is temperature), and the projection of the electric field on to the grating vector E_p.

Photorefractive response time can be explained in terms of the increased trap density evaluated; the evaluated trap density T_i values increase in the order of OXD-7 < Alq_3 < BPhen, which follows the decrease of the response time. The larger trap density is preferred for faster response time. The response time for the optical diffraction is also explained from the aspect of the photocurrent; the photocurrent increases in the order of BPhen < Alq_3 < OXD-7, which follows the increase of the response time.

Meerholz et al. defined a response time τ_G that all the traps are filled by the photo-generated holes [8]:

$$\tau_G = \frac{T_i}{\left(\frac{\alpha \eta_p I_0}{h\nu}\right)} \tag{4.5}$$

τ_G is a fundamental limit for grating formation given by the time required to generate the space-charge density that builds up the steady-state space-charge field across the grating period. This model is predicted on the assumption that all the other processes including charge transport, charge trapping and chromophore orientation arise instantaneously after the photo-generation of the PR composite. Namely, these processes lengthen the time of the grating formation.

Using the equations (4.1) and (4.2), the equation (4.5) can be simplified by the equation (4.6) :

$$\tau_G = \frac{\varepsilon_r \varepsilon_0}{\sigma_{ph}} \tag{4.6}$$

The response time τ_G is simply inversely proportional to the photoconductivity σ_{ph} and, related to the dielectric constant. Namely, equation (4.6) shows that photorefractive response is straightly correlated to the photoconductivity i.e. photocurrent. Fig 4.9 shows the plot of the response time of τ (closed circles) and τ_G (open circles) as a function of the inverse of photoconductivity, σ_{ph}^{-1}, for the PTAA-based PR composites with second electron traps. The solid line in Fig. 4.9 indicates the plots based on equation (4.6), and the dashed line is the produced line from the measured values of τ. Theoretical response time τ_G is increased with the inverse of photoconductivity, σ_{ph}^{-1}, but the measured response time τ (black solid circle in Fig. 4.9) is decreased with the inverse of photoconductivity σ_{ph}^{-1}. An intersection point between the two straight lines gives an estimated response time of 94 μs with a photoconductivity of 3.3 nS cm^{-1} for the PTAA-based PR composite.

Here, τ_G is faster than τ by one order of magnitude. For the calculation of τ_G, all the photogenerated charge carriers were assumed to contribute to the trap filling. However, the resultant values of τ suggests that not all the traps are filled by the photogenerated charge carriers in the PR composites. Here, τ was define as

$$\tau = \frac{T_i}{N_c} \tag{4.7}$$

where N_C is the total number of charge carriers trapped. Ideally, when all the photogenerated charge carriers are trapped, $N_C = \alpha\eta_p I_0/h\nu$ and $\tau = \tau_G$. From the obtained results of τ, the relation of N_C between three second electron traps, N_C (OXD-7) < N_C (Alq_3) < N_C (BPhen), is evaluated. This relation is consistent with the photocurrent relation between these traps, J_{ph} (OXD-7) > J_{ph} (Alq_3) > J_{ph} (BPhen). This means the larger trap density with lower photoconductivity provides the appropriate response time for the optical diffraction.

Table 4.3. Photocurrent and related quantities in the PTAA-based PR composites with second electron traps.

	E_0 (V μm^{-1})	I_p (μA)	J_{ph} (μA cm^{-2})	σ_{ph} (nS cm^{-1})	φ_{ph}	η_p	G	T_i (cm^{-3})	E_q (V μm^{-1})	E_{SC} (V μm^{-1})	τ (μs)	τ_G (μs)
Alq_3	60	69	3151	5.25	0.0068	0.0206	0.332	7.00×10^{14}	1.64	1.63	860	59
OXD-7	60	90	4110	6.85	0.0110	0.0268	0.411	5.65×10^{14}	1.32	1.32	997	45
BPhen	60	53	2420	4.03	0.0046	0.0158	0.290	8.00×10^{14}	1.87	1.86	397	77

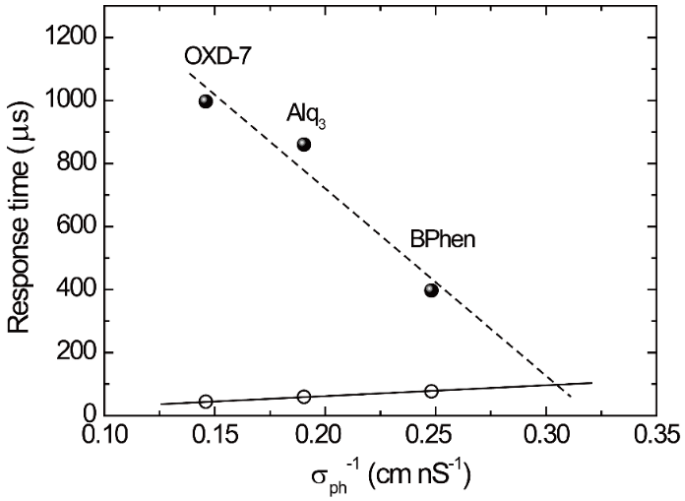

Fig. 4.10. Effect of the photocurrent on the response times τ (closed circles) and τ_G (open circles) for the PTAA-based PR composites.

4.5. Conclusion

The addition of BPhen to a PTAA-based PR composite provides high PR performance with a fast response time of 397 μs, an extremely high sensitivity of 1145 $cm^2 J^{-1}$, and a diffraction efficiency of 73.3% at 60 V μm^{-1}. The reduction of the photocurrent due to the formation of a CT complex between PTAA and BPhen significantly contributes to the appropriate formation of the space-charge field and thus the fast response time. The response time was estimated to be 94 μs with a photoconductivity of 3.3 nS cm^{-1} for the PTAA-based PR composite containing an appropriate second electron trap.

References and links

[1] C. W. Christenson, J. Thomas, P.-A. Blanche, R. Voorakaranam, R. A. Norwood, M. Yamamoto, and N. Peyghambarian, "Grating dynamics in a photorefractive polymer with Alq_3 electron traps," *Opt. Express* **18**(9), 9358–9365 (2010).

[2] J. Endres, M. Kulbak, L. Zhao, B. P. Rand, D. Cahen, G. Hodes and A. Kahn, "Electronic structure of the CsPbBr3/polytriarylamine (PTAA) system," *J. Appl. Phys.* **121**(3), 035304 (2017).

[3] X.-D. Dang, A. B. Tamayo, J. Seo, C. V. Hoven, B. Walker and T.-Q. Nguyen, "Nanostructure and optoelectronic characterization of small molecule bulk heterojunction solar cells by photoconductive atomic force microscopy," *Adv. Funct. Mater.* **20**(19), 3314–3321 (2010).

[4] Y. Shiraishi, K. Adachi, M. Itoh and T. Hirai, "Spiropyran as a selective, sensitive, and reproducible cyanide anion receptor," *Org. Lett.* **11**(15), 3482–3485 (2009).

[5] P. Chantharasupawong, C. W. Christenson, R. Philip, L. Zhai, J. Winiarz, M. Yamamoto, L. Tetard, R. R. Nair and J. Thomas, "Photorefractive performances of a graphene-doped PATPD/7-DCST/ECZ composite," *J. Mater. Chem. C Mater. Opt. Electron. Devices* **2**(36), 7639–7647 (2014).

[6] T. K. Däubler, R. Bittner, K. Meerholz, V. Cimrová and D. Neher, "Charge carrier photogeneration, trapping, and space-charge field formation in PVK-based photorefractive materials," *Phys. Rev. B* **61**(20), 13515–13527 (2000).

[7] J. S. Schildkraut and A. V. Buettner, "Theory and simulation of the formation and erasure of space charge gratings in photoconductive polymers," *J. Appl. Phys.* **72**(5), 1888–1893 (1992).

[8] T. K. Däubler, L. Kulikovsky, D. Neher, V. Cimrová, J. C. Hummelen, E. Mecher, R. Bittner and K. Meerholz, "Photoconductivity and charge-carrier photogeneration in photorefractive polymers," *Proc. SPIE* **4462**, 206–216 (2002).

Chapter 5: Optimal composition of poly(triarylamine)-based polymer composite to maximize photorefractive sensitivity

5.1. Introduction

In chapter 4, the PTAA-based PR composite with BPhen was estimated the sensitivity of over 1145 $cm^2\ J^{-1}$ as shown in Table 4.4. This extremely high sensitivity derived from the improved response time of 397 μs by adding a second electron-trapping reagent, BPhen, to control the photocurrent. However, despite the high internal diffraction efficiency above 70% is measured, the low external diffraction efficiency below 6% was observed because of the high absorption coefficient of the PTAA-based PR composites. To achieve the external diffraction efficiency greater than 10% as a requirement of holographic display system, further optimization of each composition for the PTAA-based PR composites is necessary to decrease the absorption coefficient. Above all, higher external diffraction efficiency will directly improve the sensitivity of PR composites.

In this chapter, the composition ratio of the PTAA, TAA and BPhen was optimized to obtain the enhanced PR performance. The key point of the optimization of the PTAA-based PR composite is the control of the absorption coefficient, which is related to the external diffraction efficiency.

5.2. Experimental

The detailed description about the materials and sample preparation were explained in section 2.1. PTAA as photoconductive polymer, PDCST as a NLO dye, TAA as a plasticizer, PCBM as a sensitizer and BPhen as a second electron acceptor were used (Fig. 5.1). The composition ratio of PDCST, PCBM and BPhen was fixed at 35, 0.5 and 1 by weight, respectively. The compositions of PTAA and TAA were changed to 53.5/10, 43.5/20, 33.5/30 and 23.5/40 by weight. The mixtures of the compounds were stirred in THF for 24 h and then cast on a hot plate at 70°C for 24 h. The resulting composites were sandwiched between two ITO electrodes modified with a SAM of APTMS on hot plate at 160°C. The film thickness of each PR composite was adjusted to 50 μm using Teflon spacers.

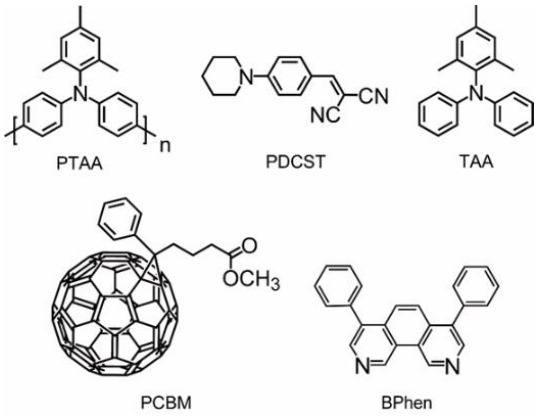

Fig. 5.1. Structural formulae of the compounds used in this chapter.

5.3. Measurements

The UV-Vis spectrum of each PR composite was measured using a Lambda1050 UV/Vis/NIR spectrophotometer (Perkin-Elmer Co., USA). The absorption coefficient α was calculated by $\alpha = A\ln(10)/d$, where A is the absorbance and d is the thickness of the PR composite.

The diffraction efficiency η and the response time τ of the PR composites was measured using a degenerate four-wave mixing (DFWM) technique. PR gratings were written in the PR device by the intersected *s*-polarized beams of a diode-pumped solid-state (DPSS) laser with λ = 532 nm (25 mW, 0.534 W cm^{-2}, Cobolt AB, Sweden). A rectangular high voltage with a 100 Hz frequency was applied to the PR device using a high-voltage amplifier (Trek 10/10E, USA). Photocurrent was simultaneously monitored using a Trek 610E high voltage amplifier when the DFWM signal was recorded.

5.4. Results and Discussion

5.4.1. Optimization of the plasticizer content for the PTAA-based PR composite

In chapter 4, by adding the second electron trap, BPhen, a sub-millisecond photorefractive response of 397 μs and a high diffraction efficiency of 73% were achieved, however, the low external diffraction efficiency of 6% was caused by the high absorption coefficient of the PTAA-based PR composite. The external diffraction efficiency is significantly influenced by the absorption coefficient at the reading wavelength of the probe beam. The UV-Vis spectrum of the PTAA and TAA in THF solution is shown in Fig. 5.2. TAA as a photoconductive plasticizer have little absorption in the visible region. On the other hand, PTAA has a broad absorption spectrum in the region of the wavelength of writing beam, 532 nm. Therefore, the content of PTAA significantly influences the absorption coefficient of the PR composite.

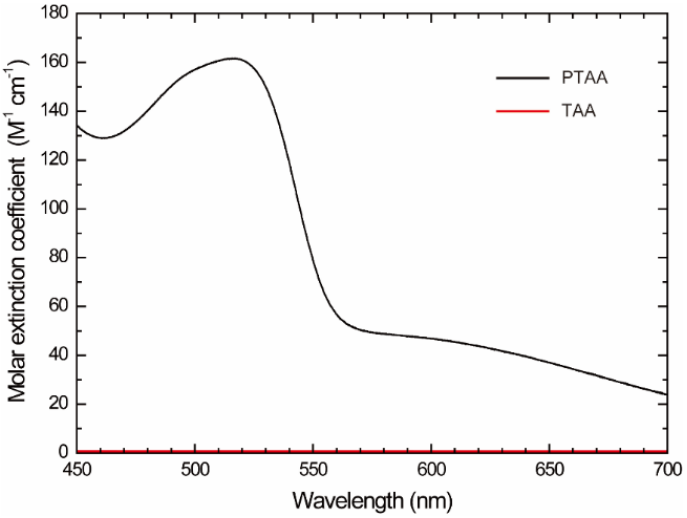

Fig. 5.2. UV-Vis absorption spectra of the PTAA and the TAA in THF solution.

The UV-Vis absorption spectra of the PTAA-based composites are shown in Fig. 5.3. With reduced content of PTAA, the absorption coefficient at 532 nm was largely decreased. Fig. 5.4 shows the photograph of each composite after one day of storage in the ambient condition. The PTAA/TAA (23.5/40) sample became opaque due to a phase separation caused by dye aggregation in the PTAA-based PR composite. The dye aggregation for this sample is caused by the low polymer content.

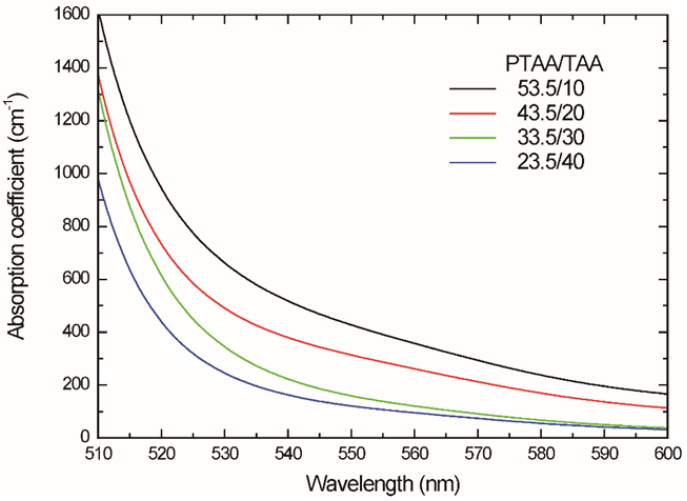

Fig. 5.3. UV-Vis absorption spectra of PTAA-based PR composites.

Fig. 5.4. Photograph of PR composites after one day of storage in the room temperature of 23°C: PTAA/TAA = (a) 53.5/10, (b) 43.5/20, (c) 33.5/30, and (d) 23.5/40.

The photocurrent plotted as a function of the electric field for the PTAA-based PR composites is shown in Fig. 5.5. The photocurrent is found to decrease with decreasing the content of PTAA which induces large photocurrent. Generally, smaller photocurrent suppresses the dielectric breakdown, however, PTAA/TAA (23.5/40) PR composite occurred dielectric breakdown at 25 V μm^{-1} due to the crystallization via dye aggregation.

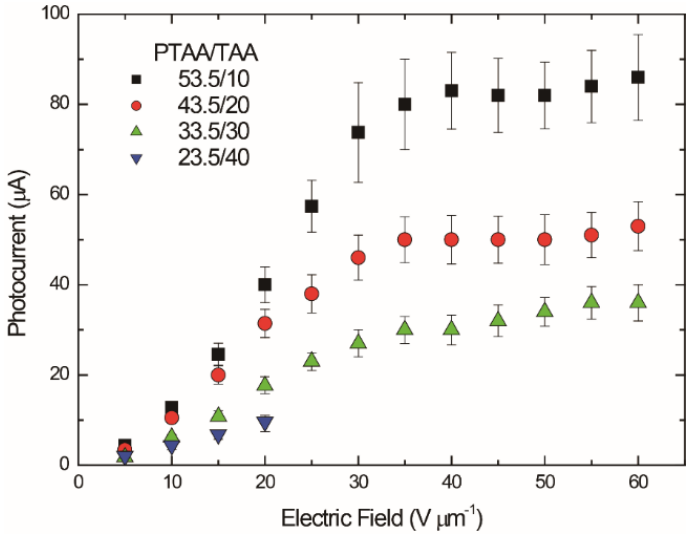

Fig. 5.5. Plots of photocurrent as a function of applied field for PTAA PR composites of PTAA/PDCST/TAA/PCBM/BPhen (53.5/35/10/0.5/1: squares, 43.5/35/20/0.5/1: circles, 33.5/35/30/0.5/1: triangles, 23.5/35/40/0.5/1: inverted triangles).

The sequence response of the diffraction efficiency was measured, applying a rectangular field with a frequency of 100 Hz (from 0 to 60 V μm^{-1}) to the PR devices. The diffraction efficiencies of PTAA/PDCST/TAA/PCBM/BPhen (53.5/35/10/0.5/1, 43.5/35/20/0.5/1, 33.5/35/30/0.5/1 by wt.) are plotted as a function of time in Fig. 5.6. The rise and decay of the diffraction efficiency corresponds to the switching on and off the applied rectangular field.

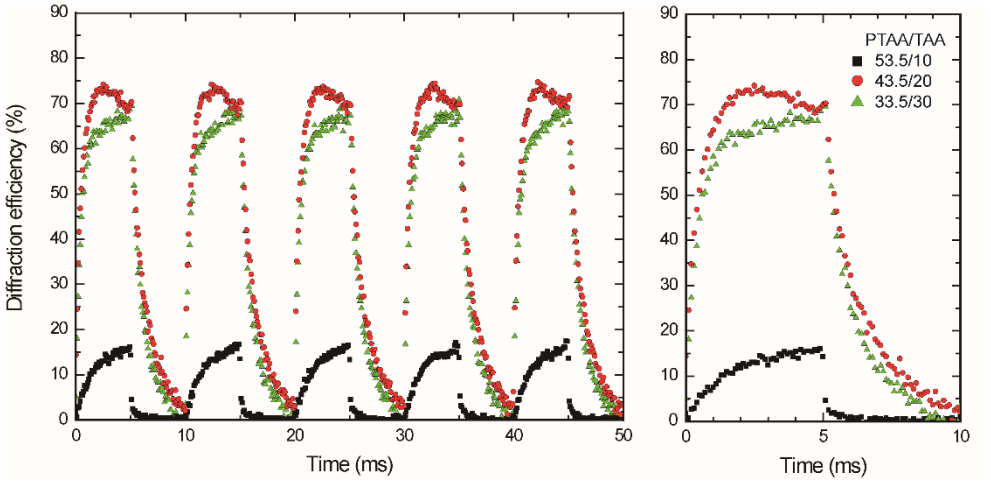

Fig. 5.6. Left: sequence response of the diffraction efficiency for the PR composites, PTAA/TAA = 53.5/10 (solid squares), 43.5/20 (solid circles) and 33.5/30 (solid triangles), applying a rectangular field at a frequency of 100 Hz (from 0 to 60 V μm^{-1}). Right: one cycle response.

The PR quantities of the PTAA-based composites are listed in Table 5.1. The diffraction efficiencies were 16.8, 73.3, and 66.5% for the PTAA/TAA (53.5/10), PTAA/TAA (43.5/20), and PTAA/TAA (33.5/30), respectively. And, the external diffraction efficiencies were 0.6, 5.9, and 12.1%, respectively. Here, the external diffraction efficiency of the PTAA/TAA (33.5/30) was twice as large as that of the PTAA/TAA (43.5/20). This difference is caused by the lower absorption coefficient of the PTAA/TAA (33.5/30). The PR response times of PTAA/TAA (33.5/30) and PTAA/TAA (43.5/20) were comparable and measured to be 422 and 397 μs, respectively. The maximum sensitivity of the PTAA/TAA (33.5/30) was estimated to be 1541 $cm^2\ J^{-1}$. The short response time and the high external diffraction efficiency resulted in the high sensitivity.

Table 5.1. PR parameters for the PTAA-based composites with various contents of TAA.

PTAA/TAA (wt%)	α (cm^{-1})	Δn	Γ (cm^{-1})	η / η_{ext} (%)	τ (μs) / β	S ($cm^2\ J^{-1}$)
53.5/10	625	1.28×10^{-3}	63	16.8 / 0.6	1578 / 0.93	89
43.5/20	462	3.13×10^{-3}	156	73.3 / 5.9	397 / 0.54	1145
33.5/30	313	2.90×10^{-3}	215	66.5 / 12.1	422 / 0.98	1541
23.5/40	223			—*		

*Dielectric breakdown below 25 V μm^{-1}

5.4.2. Photorefractive response and photocurrent

The photoconductive parameters related to the photocurrent and PR quantities in the PTAA-based PR composites are listed in Table 5.2. The procedures to calculate these parameters and quantities were described in the Chapter 4.

Table 5.2. Photocurrent and related quantities in the PR composites with various contents of TAA.

PTAA/TAA (wt%)	E_0 (V μm^{-1})	I_p (μA)	J_{ph} (μA cm^{-2})	σ_{ph} (nS cm^{-1})	φ_{ph}	η_p	G	T_i (cm^{-3})	E_q (V μm^{-1})	E_{SC} (V μm^{-1})	τ (μs)	τ_G (μs)	N_c (s^{-1} cm^{-3})
53.5/10	60	86	3927	6.54	0.0063	0.0256	0.245	9.48×10^{14}	2.3	2.3	1578	47	6.0×10^{17}
43.5/20	60	53	2420	4.03	0.0046	0.0158	0.290	8.00×10^{14}	1.9	1.9	397	77	2.0×10^{18}
33.5/30	60	36	1644	2.74	0.0046	0.0107	0.428	5.42×10^{14}	1.3	1.3	422	113	1.3×10^{18}

In the present case, the total number of charge carriers trapped N_C is used to evaluate the PTAA/TAA contents dependence on the response time for the PTAA-based PR composites. N_C is as follows; N_C (PTAA/TAA (53.5/10)) < N_C (PTAA/TAA (33.5/30)) < N_C (PTAA/TAA (43.5/20)). The estimated N_C shows that higher PTAA content leads to lower trap density. This result contradicts the common understanding for trap density in polymers. N_C of polymers is commonly higher than that for monomeric materials with low molecular weight, therefore, the N_C of the PR composite with higher content of PTAA should be higher. So, another reasonable explanation should be considered.

Generally, the energy distribution of hopping sites in polymer is broader compared to the corresponding monomeric low molecular weight compound. Therefore, the electronic density of state (DOS) of hopping sites becomes wider for the polymer-rich PR composite. In a previous study [1], narrower DOS led to the shorter response time, whereas wider DOS led to the longer response time for the PR composite of poly(4-(diphenylamino)benzylacrylate) (PDAA) as a photoconductive polymer and (4-(diphenylamino)phenyl)methanol (TPAOH) as a plasticizer. TPAOH is a monomeric unit of PDAA, i.e., the decrease of PDAA content contributed to narrower DOS bandwidth. The narrower DOS distribution led the faster response time. The similarity between PTAA/TAA and PDAA/TPAOH assumes that the same phenomenon occurs in the PTAA/TAA based PR composite. The predicted energy distribution of hopping sites for the PTAA/TAA composite is shown in Fig. 5.7. A higher content of PTAA in the case of PTAA/TAA (53.5/10) results in a wider distribution of DOS, leading to the slower response of diffraction. In contrast, the lower content of PTAA in the case of PTAA/TAA (43.5/20) and PTAA/TAA (33.5/30) gives a narrower distribution of DOS, leading to the faster response of diffraction. The PR diffraction responses of PTAA/TAA (43.5/20) and PTAA/TAA (33.5/30) were nearly equivalent; thus, 20 wt% of TAA is sufficient for forming a narrower distribution of DOS in PTAA/TAA PR composite.

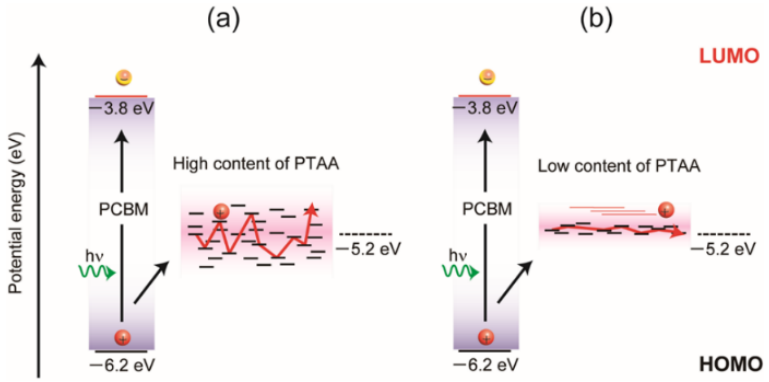

Fig. 5.7. Hole-drafting mechanism of PTAA-based PR composite: (a) composite with high content of PTAA, (b) composite with low content of PTAA.

5.4.3. Optimization of the second electron trap content for the PTAA-based PR composites

For further optimization of the PTAA/TAA based PR composites, the effect of the BPhen content on PR performances is investigated. In the Chapter 4, by adding the second electron trap, BPhen on a PTAA-based PR composites, a sub-millisecond photorefractive response was achieved with decreasing photocurrent. Adding a higher content of BPhen with decreasing the content of PTAA was expected to be faster response time with lower absorption coefficient and photocurrent.

The PR parameters of the PTAA-based PR composites are listed when the content of BPhen is changed from 1 to 5 wt% in Table 5.3. Increasing the content of BPhen, the absorption coefficient and the photocurrent of PTAA-based PR composites are decreased. The obtained results of η_{ext}, τ and S are plotted as a function of BPhen content in Fig. 5.8. η_{ext} is increased with increasing content of BPhen, and longer τ is measured. A maximum sensitivity of 1851 $cm^2\ J^{-1}$ is measured for PTAA/PDCST/TAA/PCBM/BPhen (31.5/35/30/0.5/3 by wt.).

Table 5.3. PR quantities and parameters in the PTAA-based composites with various contents of BPhen.

BPhen content (wt%)	α (cm^{-1})	I_p (μA)	Δn	η (η_{ext}) (%)	τ (μs) / β	S ($cm^2\ J^{-1}$)
1	313	36	2.90×10^{-3}	66.5 (12.1)	422 / 0.98	1541
3	205	22	3.12×10^{-3}	73.1 (23.9)	494 / 0.98	1851
5	191	14	3.14×10^{-3}	73.7 (26.0)	573 / 0.98	1664

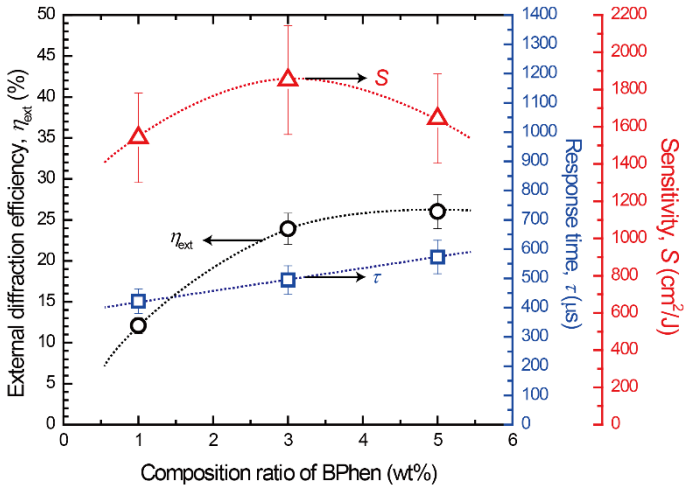

Fig. 5.8. Plots of external diffraction efficiency, response time, and sensitivity as a function of BPhen content under a rectangular applied field at a frequency of 100 Hz (from 0 to 60 V μm^{-1}).

5.5. Conclusion

The effects of the composition of each component of PR composites were investigated for PTAA/PDCST/TAA/PCBM/BPhen on the PR performance from the perspective of improving the external diffraction efficiency and the sensitivity. By optimizing the contents of TAA and BPhen, higher PR performances were achieved: response time of 494 μs, external diffraction efficiency of 23.9%, and sensitivity of 1851 cm^2 J^{-1} at 60 V μm^{-1} for PTAA/PDCST/TAA/PCBM/BPhen (31.5/35/30/0.5/3 by wt.). The high external diffraction efficiency was caused by the reduction of the absorption coefficient of the PTAA-based PR composite by decreasing the contents of PTAA and increasing the contents of TAA and BPhen. The small content of PTAA also contributed to the short response time by forming a narrower DOS distribution.

References and links

[1] T. V. Nguyen, K. Kinashi, W. Sakai and N. Tsutsumi, "Enhanced photorefractivity of a perylene bisimide-sensitized poly(4-(diphenylamino)benzyl acrylate) composite," *Opt. Material Express* **6**(5), 1714-1723 (2016).

Chapter 6: Summary

The Photorefractive (PR) effect is defined as spatial modulation of the index of refraction due to charge redistribution in a nonlinear optical material. Holographic displays using the PR effect have received a great deal of attention because they can essentially provide 3D images without special eyeglasses. For practical use of the PR polymer materials, the high external diffraction efficiency and fast response of the PR polymer composites are indispensable.

This thesis consists of six chapters, featuring PR dynamics in poly(triarylamine) (PTAA) based polymer composite from chapter 3 to chapter 5.

In chapter 1, as an introduction, history of the studies related to the PR materials was presented. Through the history, PR response was focused on as one of the wishes to improve. In this study, PTAA was chosen as a PR photoconductive polymer, which is expected to lead fast response due to its high hole mobility ($\mu = 10^{-3}$-10^{-2} cm^2 V^{-1} s^{-1}).

In chapter 2, as an experimental section, materials and composite preparation including synthetic procedures, and measurement were presented.

In chapter 3, the PR performance of a PTAA-based PR polymer composite was improved by optimizing the content of sensitizer. The diffraction efficiency as a function of applied field demonstrated appropriate applied field region of 45-60 V μm^{-1}. Wavelength dependency of the PR performance was also examined. The shorter wavelength illumination induced higher PR diffraction efficiency and faster response time due to the appropriate charge generation. The basic experimental conditions for PTAA-based PR polymer composite, applied field of 45-60 V μm^{-1} and 532 nm illumination, were settled.

In chapter 4, the PR dynamics of PTAA-based composite with small amount of a second electron acceptor was investigated. The 532 nm illumination led high PR performance in the chapter 3, however, high photocurrent sparking dielectric breakdown was observed. As second electron trap agents, tris(8-hydroxyquinolinato)aluminium (Alq_3), 1,3-bis[2-(4-tert-butylphenyl)-1,3,4-oxadiazo-5-yl]benzene (OXD-7) and bathophenanthroline (BPhen) were introduced to the PTAA-based PR polymer composite, respectively. The second electron trap agents reduced photocurrent and suppressed the dielectric breakdown despite the high applying electric field of 60 V μm^{-1}. Remarkably, the addition of BPhen to a PTAA-based PR composite provided high PR performance with a fast response time of 397 μs, an extremely high sensitivity of 1145 cm^2 J^{-1}, and a diffraction efficiency of 73.3% at 60 V μm^{-1}. The reduction of the photocurrent due to the formation of a CT complex between PTAA and BPhen significantly contributes to the appropriate formation of the space-charge field and thus the fast response time. From the photoconductive properties in the PTAA-based PR composite, the response time was estimated to be 94 μs with a photoconductivity of 3.3 nS cm^{-1} for the PTAA-based PR composite containing an appropriate second electron trap.

In chapter 5, the composition ratio was optimized to obtain the enhanced PR performance. The high PR performance was induced by adding a second electron-trapping reagent, BPhen, however, the low external diffraction efficiency below 6% was observed because of the high absorption coefficient of the PTAA-based PR composites. To achieve the criteria of holographic display system, external diffraction efficiency greater than 10% is necessary. By optimizing the contents of TAA and BPhen, higher external diffraction efficiency and sensitivity were achieved: response time of 494 μs, external diffraction efficiency of 23.9%, and sensitivity of 1851 $cm^2 J^{-1}$ for PTAA/PDCST/TAA/PCBM/BPhen (31.5/35/30/0.5/3 by wt.). The reduction of the PTAA content with increasing the content of TAA and BPhen led the smaller absorption coefficient and resulting higher external diffraction efficiency. The low content of PTAA contributed to the short response time by forming a narrower DOS distribution.

From the study of chapter 3-5, the PR performance of the PTAA-based PR composite has significantly improved satisfying the criteria of holographic display. As new findings, not only the improvement method of the PR performance, but also the PR dynamics related to the photocurrent induced by PTAA were discussed.

List of publication

Chapter 3

N. Tsutsumi, K. Kinashi, K. Masumura, and K. Kono, “Photorefractive performance of poly(triarylamine)-based polymer composites: An approach from the photoconductive properties,” *J. Polym. Sci., B, Polym. Phys.* **53**(7), 502–508 (2015).

Chapter 4

N. Tsutsumi, K. Kinashi, K. Masumura, and K. Kono, “Photorefractive dynamics in poly(triarylamine)-based polymer composites,” *Opt. Express* **23**(19), 25158-25170 (2015).

K. Masumura, T. Oka, K. Kinashi, and N. Tsutsumi, “Photorefractive dynamics in poly(triarylamine)-based polymer composite: An approach utilizing a second electron trap to reduce the photoconductivity,” *Opt. Material Express* **8**(22), 401-412 (2018).

Chapter 5

K. Masumura, I. Nakanishi, K. V. T. Khuat, K. Kinashi, W. Sakai and N. Tsutsumi, “Optimal composition of the poly(triarylamine)-based polymer composite to maximize Photorefractive performance,” *Sci. Rep.*, **9**, 739 (2019).

Acknowledgements

This thesis has been carried out under the direction of Professor Naoto Tsutsumi at Faculty of Materials Science and Engineering in Kyoto Institute of Technology. I would like to express my deepest gratitude to Professor Naoto Tsutsumi for his comprehensive guidance and kind support. He taught me the pleasure of discovering new phenomena and materials, throughout the period of bachelor's program and master's program for 2012-2015, and doctor's program for 2016-2018.

I express thanks to Associate Professor Wataru Sakai and Assistance Professor Kenji Kinashi at Faculty of Materials Science and Engineering in Kyoto Institute of Technology for their advice and discussion. Associate Professor Wataru Sakai taught me the importance of taking an objective view of own study. Professor Kenji Kinashiri gave me experiment techniques of organic synthesis and polymerization.

This study would be impossible without the supports from the members of Functional Polymer Design Laboratory, Professor Tsutsumi's group. I particularly thank to Mr. Tsuyoshi Oka, Mr. Ikumi Nakanishi, Ms. Khanh Van Thi Khuat. They all kindly prepared the experimental samples and discuss the research at any time despite being busy.

Finally, I wish to thank to my wife, Mayu, for understanding my work and giving continuous support and encouragement.